Effects of gap anisotropy upon the electronic structure around a superconducting vortex

Nobuhiko Hayashi, Masanori Ichioka, and Kazushige Machida
Department of Physics, Okayama University, Okayama 700, Japan
(May 2, 1997)

An isolated single vortex is considered within the framework of the quasiclassical theory. The local density of states around a vortex is calculated in a clean type II superconductor with an anisotropy. The anisotropy of a superconducting energy gap is crucial for bound states around a vortex. A characteristic structure of the local density of states, observed in the layered hexagonal superconductor $2H$-$NbSe_2$ by scanning tunneling microscopy (STM), is well reproduced if one assumes an *anisotropic* s-wave gap in the hexagonal plane. The local density of states (or the bound states) around the vortex is interpreted in terms of quasiparticle trajectories to facilitate an understanding of the rich electronic structure observed in STM experiments. It is pointed out that further fine structures and extra peaks in the local density of states should be observed by STM.

PACS number(s): 74.60.Ec, 61.16.Ch, 74.25.Jb

I. INTRODUCTION

Recently, the existence of an anisotropy of a superconducting energy gap has attracted a great deal of attention in various superconductors such as heavy Fermion, organic, and high T_c compounds. On the other hand, the electronic structure around vortices is a fundamental problem on the physics of both conventional and unconventional superconductors. In this paper, we discuss effects of the gap anisotropy upon the electronic structure around a vortex, i.e., the bound states around an isolated vortex in clean type II superconductors.

Theoretically, the bound states around a vortex was discussed in 1964 by Caroli, de Gennes, and Matricon,[1] who considered a single vortex in an isotropic s-wave superconductor. After this work, several theorists studied the electronic structure around vortices.[2–5] Experimentally, however, until the following success by Hess *et al.*, there had existed for a long time no experiments which could directly study the electronic structure around vortices.[6]

In 1989, a novel experimental method, scanning tunneling microscopy (STM), opened up a way to the study of the electronic structure around vortices in type II superconductors.[6,7] Using the STM method, Hess *et al.*[8] succeeded in measuring spatially resolved excitation spectra, i.e., local density of states (LDOS) around a vortex. They investigated the bound states around a vortex in the layered hexagonal compound $2H$-$NbSe_2$ (T_c=7.2 K), and found a striking zero-bias peak at the vortex center. The same peak and its collapse upon substituting Ta for Nb as impurities in $NbSe_2$ were also observed by Renner *et al.*[9] Several new theoretical studies of the electronic structure around a vortex[10–18] were prompted by the success of the STM experiment by Hess *et al.*[8] Some of these theories[12,14–17] predicted that the zero-bias peak should split into two, i.e., into positive and negative bias voltage peaks, if spectra are taken at some distance from the vortex center (see, for instance, Fig. 3 in Ref. 12). This splitting indicates that quasiparticles of the vortex bound states with finite angular momentum are distributed circularly, and circulate farther away from the core center as they have higher energy. The predicted splitting was actually confirmed in an experiment.[19]

However, a mystery also emerged. In the above experiment, Hess *et al.*[19] not only confirmed the splitting, but also found that the LDOS around the vortex was shaped like "star" at a fixed energy and its orientation was dependent on the energy, i.e., the sixfold star shape rotates as the bias voltage varies. (Fig. 4 in Ref. 19.) Soon after this observation was made, Gygi and Schlüter[20] proposed an explanation for this 30° rotation of the star-shaped LDOS. On the basis of a sixfold perturbation, they explained that the two states, i.e., the lower and higher energy stars were interpreted as bonding or antibonding states.[20] Although they explained certain aspects of the observation, the following features of the star-shaped LDOS observed in later experiments[21,22,7,23] could not be sufficiently understood by this perturbation scheme. In the intermediate energy, a "ray" of the star splits into a pair of nearly parallel rays.[21,22] (Fig. 1 in Ref. 21 or Fig. 1 in Ref. 22.) The zero-bias peak in the spectral evolution along a radial line from the vortex center does not split into two subpeaks observed in the earlier experiment, but into three or more ones.[7,23] (Figs. 9 and 10 in Ref. 7, or Fig. 6 in Ref. 23.)

Specifically, the characteristic features of the LDOS observed in $NbSe_2$[19,21,22,7,23] are summarized in detail as follows, when the magnetic field H is applied perpendicular to the hexagonal plane: (1) The LDOS for quasiparticle excitations has a sixfold star shape centered at the vortex center.[19] (2) The orientation of this star depends on the energy. At zero bias, a ray of the star extends away from the a axis in the hexagonal plane of $NbSe_2$. Upon increasing the bias voltage, the star rotates by 30°. (3) In the intermediate bias voltage, a ray splits into a pair of nearly parallel rays, keeping its direction fixed.[21,22] (4) In the spectral evolution which crosses

the vortex center, there exist inner peaks in addition to the outer peaks which evolve from the zero bias peak at the vortex center into the bulk BCS like gap edges far from the vortex.[7,23] The inner peaks vary with the angle of the direction in which the spectral evolution is taken. These important and interesting observations (1)–(4) remain unexplained.

Quite recently, motivated by a possibility of a d-wave superconductivity in high T_c cuprates, Schopohl and Maki[24,25] studied the electronic structure around a vortex in a d-wave superconductor. On the basis of the quasiclassical Green's function theory,[26–28] the LDOS around a single vortex was calculated in a superconductor with a d-wave energy gap. They found that the LDOS exhibits a characteristic fourfold structure in the d-wave gap case, which is contrasted with the isotropic s-wave gap case (a circularly symmetric LDOS).[24,25] A gradual 45° rotation of this fourfold LDOS as the energy changes was later reported by the present authors.[29] We note that this rotation is similar to that observed in $NbSe_2$.[30]

In the context described above, we have investigated the electronic structure around the vortex observed in $NbSe_2$. We find that the rich structure of the LDOS observed in the STM experiments[19,21,22,7,23] results mainly from a superconducting gap anisotropy. Assuming an *anisotropic* s-wave gap analogous to the d-wave one, we are able to obtain results favorably comparable with the experiments. In a previous short paper,[31] we enumerated the following items as the possible origin of the rich structure of the LDOS: (a) the effect of an anisotropic superconducting energy gap, (b) the effect of nearest-neighbor vortices, i.e., the effect of the vortex lattice, and (c) the effect of the anisotropic density of states at the Fermi surface. It is the purpose of the present paper to discuss the gap effect (a) in more detail. As for the item (b), i.e., the vortex lattice effect, we gave a detailed report in Ref. 32. A detailed report for (c) the effect of the anisotropic density of states at the Fermi surface is given elsewhere.[33]

To date, $NbSe_2$ has been the only compound in which the electronic structure around vortices was thoroughly investigated by STM. In this paper, we concentrate our attention on the LDOS observed in $NbSe_2$ as a typical example of a type II superconductor. However, the essence of the present considerations is equally applicable to other type II superconductors in general. The LDOS around a vortex reflects the internal electronic structure of the vortex, and an understanding of this structure is important in elucidating dynamical properties of vortices as well as static ones.

We consider the case of an isolated static vortex under a magnetic field applied parallel to the c axis (or z axis). We restrict ourselves to a two dimensional system, i.e., assume a two dimensional Fermi surface neglecting a small warping of the Fermi surface along the c axis, which is appropriate to layered superconductors such as $NbSe_2$.[34,35]

In Sec. II, we describe the quasiclassical theory we use for the study of the vortex. Section III is devoted to the calculations of the LDOS around a vortex under the influence of the gap anisotropy. In Sec. IV, we interpret the resultant LDOS in terms of quasiparticle trajectories. The summary and discussions are given in Sec. V.

II. THE QUASICLASSICAL THEORY

To investigate the LDOS around a vortex, we use the quasiclassical Green's function theory.[26–28] The quasiclassical theory is a very powerful method, especially for spatially inhomogeneous systems such as surfaces[36,37] and vortices.[38,39] Furthermore, one can easily treat a superconducting gap anisotropy as well as the Fermi surface anisotropy in the quasiclassical theory. We consider the transportlike Eilenberger equation for the quasiclassical Green's function

$$\hat{g}(i\omega_n,\mathbf{r},\bar{\mathbf{k}}) = -i\pi \begin{pmatrix} g(i\omega_n,\mathbf{r},\bar{\mathbf{k}}) & if(i\omega_n,\mathbf{r},\bar{\mathbf{k}}) \\ -if^{\dagger}(i\omega_n,\mathbf{r},\bar{\mathbf{k}}) & -g(i\omega_n,\mathbf{r},\bar{\mathbf{k}}) \end{pmatrix} \tag{2.1}$$

in a 2×2 matrix form (for even-parity superconductivity), namely,

$$i\mathbf{v}_{\mathrm{F}}(\bar{\mathbf{k}})\cdot\nabla\hat{g}(i\omega_n,\mathbf{r},\bar{\mathbf{k}}) + \left[\begin{pmatrix} i\omega_n & -\Delta(\mathbf{r},\bar{\mathbf{k}}) \\ \Delta^*(\mathbf{r},\bar{\mathbf{k}}) & -i\omega_n \end{pmatrix},\ \hat{g}(i\omega_n,\mathbf{r},\bar{\mathbf{k}})\right] = 0. \tag{2.2}$$

The Eilenberger equation (2.2) is supplemented by the normalization condition

$$\hat{g}(i\omega_n,\mathbf{r},\bar{\mathbf{k}})^2 = -\pi^2\hat{1}. \tag{2.3}$$

Here $\omega_n = (2n+1)\pi T$ is the Matsubara frequency. The vector $\mathbf{r} = (x,y)$ is the center of mass coordinate, and the unit vector $\bar{\mathbf{k}}$ represents the relative coordinate of the Cooper pair. The overbar denotes unit vectors. The commutator $[\hat{A},\hat{B}] = \hat{A}\hat{B} - \hat{B}\hat{A}$. We assume the Fermi velocity $\mathbf{v}_{\mathrm{F}}(\bar{\mathbf{k}})$ is a function of $\bar{\mathbf{k}}$ with reflecting the anisotropy of the Fermi surface. Since we consider an isolated single vortex in an extreme type II superconductor where the Ginzburg-Landau parameter $\kappa \gg 1$, the vector potential can be neglected in Eq. (2.2).

The Eilenberger equation in the matrix form (2.2) can be written down to the following equations,

$$\left(\omega_n + \frac{v_{\mathrm{F}}(\theta)}{2}\frac{d}{dr_{\parallel}}\right) f(i\omega_n,\mathbf{r},\theta) = \Delta(\mathbf{r},\theta)g(i\omega_n,\mathbf{r},\theta), \tag{2.4a}$$

$$\left(\omega_n - \frac{v_{\mathrm{F}}(\theta)}{2}\frac{d}{dr_{\parallel}}\right) f^{\dagger}(i\omega_n,\mathbf{r},\theta) = \Delta^*(\mathbf{r},\theta)g(i\omega_n,\mathbf{r},\theta), \tag{2.4b}$$

$$v_{\rm F}(\theta)\frac{d}{dr_\parallel}g(i\omega_n,\mathbf{r},\theta)=\Delta^*(\mathbf{r},\theta)f(i\omega_n,\mathbf{r},\theta) - \Delta(\mathbf{r},\theta)f^\dagger(i\omega_n,\mathbf{r},\theta), \quad (2.4c)$$

which are supplemented by

$$g(i\omega_n,\mathbf{r},\theta)=[1-f(i\omega_n,\mathbf{r},\theta)f^\dagger(i\omega_n,\mathbf{r},\theta)]^{1/2}, \quad \mathrm{Re}\ g(i\omega_n,\mathbf{r},\theta)>0. \quad (2.5)$$

Here, $\bar{\mathbf{k}}=(\cos\theta,\sin\theta)$,

$$\mathbf{v}_{\rm F}(\bar{\mathbf{k}})=\big(|\mathbf{v}_{\rm F}(\theta)|\cos\Theta(\theta),|\mathbf{v}_{\rm F}(\theta)|\sin\Theta(\theta)\big) =\big(v_{\rm F}(\theta)\cos\Theta(\theta),v_{\rm F}(\theta)\sin\Theta(\theta)\big), \quad (2.6)$$

and the following coordinate system is taken: $\bar{\mathbf{u}}=\cos\Theta\bar{\mathbf{x}}+\sin\Theta\bar{\mathbf{y}}$, $\bar{\mathbf{v}}=-\sin\Theta\bar{\mathbf{x}}+\cos\Theta\bar{\mathbf{y}}$, and thus a point $\mathbf{r}=x\bar{\mathbf{x}}+y\bar{\mathbf{y}}$ is denoted as $\mathbf{r}=r_\parallel\bar{\mathbf{u}}+r_\perp\bar{\mathbf{v}}$. The center of a vortex line is situated at the origin $\mathbf{r}=(0,0)$. The angle θ, i.e., the direction of $\bar{\mathbf{k}}$ is measured from the a axis (or x axis) in the hexagonal plane of $NbSe_2$. If one considers a cylindrical Fermi surface with anisotropic Fermi velocity, then $\mathbf{v}_{\rm F}(\bar{\mathbf{k}})=v_{\rm F}(\theta)\bar{\mathbf{k}}=\big(v_{\rm F}(\theta)\cos\theta,v_{\rm F}(\theta)\sin\theta\big)$.

The self-consistent equation is given by

$$\Delta(\mathbf{r},\theta)=N_0 2\pi T\sum_{\omega_n>0}\int_0^{2\pi}\frac{d\theta'}{2\pi}\rho(\theta')V(\theta,\theta')f(i\omega_n,\mathbf{r},\theta'), \quad (2.7)$$

where N_0 is the total density of states over the Fermi surface in the normal state. The θ-dependence of the density of states at the Fermi surface is represented by

$$\rho(\theta)=\frac{1}{N_0|\bar{\mathbf{k}}\cdot\mathbf{v}_{\rm F}(\bar{\mathbf{k}})|}, \quad (2.8)$$

which satisfies $\int(d\theta/2\pi)\rho(\theta)=1$. We assume that the pairing interaction $V(\theta,\theta')$ is separable, i.e., $V(\theta,\theta')=vF(\theta)F(\theta')$, where v is the strength of the pairing interaction and $F(\theta)$ is a symmetry function, e.g., $F(\theta)=\cos 2\theta$ for a d-wave pairing, $F(\theta)=1$ for an isotropic s-wave pairing, etc.

The pair potential is written as

$$\Delta(\mathbf{r},\theta)=\Delta(\mathbf{r})F(\theta). \quad (2.9)$$

To obtain a self-consistent pair potential, we solve Eqs. (2.4) and (2.7) iteratively. This computation is performed after a method of Ref. 29. In the calculation of the pair potential, we adopt the so-called explosion method[40,41] to solve Eq. (2.4).

The LDOS is evaluated from

$$N(E,\mathbf{r})=N_0\int_0^{2\pi}\frac{d\theta}{2\pi}\rho(\theta)\mathrm{Re}\ g(i\omega_n\to E+i\eta,\mathbf{r},\theta) \equiv\int_0^{2\pi}\frac{d\theta}{2\pi}\rho(\theta)N(E,\mathbf{r},\theta), \quad (2.10)$$

where η (>0) is a small real constant. The value of η represents the effect of dilute impurities in a rough approximation[16,18] or other smearing effects.[42] To obtain $g(i\omega_n\to E+i\eta,\mathbf{r},\theta)$, we have to solve Eq. (2.4) for $\eta-iE$ instead of the Matsubara frequency ω_n. While we succeeded in this calculation in the vortex lattice case with the explosion method, a huge computer-running-time for the numerical calculation was needed in this method.[32] In the case of the isolated single vortex, however, it is convenient to utilize a method of the Riccati equation developed by Schopohl.[24,25,43] The Riccati equation simplifies the numerical computation.

The Riccati equations[24] are given as

$$v_{\rm F}(\theta)\frac{d}{dr_\parallel}a(\omega_n,\mathbf{r},\theta)-\Delta(\mathbf{r},\theta) +\Big(2\omega_n+\Delta^*(\mathbf{r},\theta)a(\omega_n,\mathbf{r},\theta)\Big)a(\omega_n,\mathbf{r},\theta)=0, \quad (2.11)$$

$$v_{\rm F}(\theta)\frac{d}{dr_\parallel}b(\omega_n,\mathbf{r},\theta)+\Delta^*(\mathbf{r},\theta) -\Big(2\omega_n+\Delta(\mathbf{r},\theta)b(\omega_n,\mathbf{r},\theta)\Big)b(\omega_n,\mathbf{r},\theta)=0. \quad (2.12)$$

Equations (2.11) and (2.12) are obtained by substituting the following parametrizations[24] into the Eilenberger equation (2.4),

$$f=\frac{2a}{1+ab},\quad f^\dagger=\frac{2b}{1+ab},\quad g=\frac{1-ab}{1+ab}. \quad (2.13)$$

We solve Eqs. (2.11) and (2.12) independently along the $r_\parallel$-trajectory where $r_\perp$ is held constant. In the isolated single vortex under consideration, one can integrate Eqs. (2.11) and (2.12) using solutions far from the vortex,

$$a_{-\infty}=\frac{\sqrt{\omega_n^2+|\Delta(-\infty,r_\perp,\theta)|^2}-\omega_n}{\Delta^*(-\infty,r_\perp,\theta)},$$
$$b_{+\infty}=\frac{\sqrt{\omega_n^2+|\Delta(+\infty,r_\perp,\theta)|^2}-\omega_n}{\Delta(+\infty,r_\perp,\theta)}\quad(\omega_n>0) \quad (2.14)$$

as the initial values, respectively.[43] There, to remove the exploding solution, the integral about a is performed from $r_\parallel=-\infty$, and about b from $r_\parallel=+\infty$.[43] We numerically integrate the first-order differential equations (2.11) and (2.12) by the adaptive stepsize control Runge-Kutta method.[44] The Green's function $g(i\omega_n\to E+i\eta,\mathbf{r},\theta)$ is obtained from Eq. (2.13) if one solves Eqs. (2.11) and (2.12) for $\eta-iE$ instead of ω_n. When we solve Eqs. (2.11) and (2.12) for $\eta-iE$, we use the self-consistently obtained pair potential $\Delta(\mathbf{r})$ which is calculated beforehand.

From now on, the density of states, energies, and lengths are measured in units of N_0, the uniform gap Δ_0 at the temperature $T=0$, and the coherence length $\xi_0=v_{\rm F0}/\Delta_0$ ($v_{\rm F0}\equiv 1/N_0$), respectively.

III. PAIR POTENTIAL AND LOCAL DENSITY OF STATES

Before going into technical details, we briefly explain our model and its parameter involved in connection with $NbSe_2$, which is a typical type II s-wave superconductor. We assume the following model of an anisotropic s-wave pairing in Eq. (2.9),

$$F(\theta) = 1 + c_{\rm A} \cos 6\theta. \tag{3.1}$$

Here we again stress that the angle θ, i.e., the direction of $\bar{\mathbf{k}}$ is measured from the a axis (or x axis) in the hexagonal plane of $NbSe_2$. Thus the parameter $c_{\rm A}$ denotes the degree of anisotropy in the superconducting energy gap.[45–47] The case $c_{\rm A} = 0$ corresponds to a conventional isotropic gap.

The anisotropic s-wave gap is certainly suggested in $NbSe_2$ from a scanning tunneling spectroscopy (STS) experiment at zero field.[23] The I-V tunneling spectrum, observed at the extreme low temperature $T = 50$ mK, indicates a substantial gap anisotropy (the gap amplitude with the averaged value 1.1 meV distributes from 0.7 to 1.4 meV, see Fig. 1 in Ref. 23), which is consistent with the density of states in the anisotropic s-wave gap case [Fig. 1]. It is seen from Fig. 1 that the gap edge distributes from $E = 1 - c_{\rm A}$ to $1 + c_{\rm A}$ in the case of the anisotropic gap. Then, the experimental data of STS[23] indicate that $c_{\rm A} \sim 1/3$. Similarly, a nuclear quadrupole resonance, NQR, experiment[48] in $NbSe_2$ suggests an anisotropic s-wave energy gap. The temperature dependence of the spin-lattice relaxation rate $1/T_1$ is well fitted by an anisotropic energy gap model following Hebel[49] with the value of a parameter $\delta/\Delta(0) \sim 1/3$.[48] Here the broadening in the gap edge, $\delta/\Delta(0)$, of Ref. 48 corresponds to $\delta/\eta_0(0)$ of Ref. 49. This parameter $\delta/\Delta(0)$ corresponds well to our parameter of the gap anisotropy, $c_{\rm A}$, because both parameters δ and $c_{\rm A}$ yield the broadening in the gap edge. We set $c_{\rm A} = 1/3$ as a representative case in the following.

In this paper, we restrict our attention to the gap anisotropy effect only, neglecting other effects, i.e., the vortex lattice effect and the effect of the anisotropic density of states at the Fermi surface, to clearly see how the energy gap anisotropy influences the LDOS. We calculate the LDOS in the isolated vortex case assuming an isotropic cylindrical Fermi surface ($\mathbf{v}_{\rm F}(\bar{\mathbf{k}}) \parallel \bar{\mathbf{k}}$, $v_{\rm F}(\theta) = v_{\rm F0}$).

A. Pair potential

In order to calculate the LDOS, we need the self-consistent pair potential obtained at the temperature, say, $T = 0.1T_c$ (T_c is the superconducting transition temperature). The self-consistently obtained real-space variation part of the pair potential, $\Delta(\mathbf{r})$, certainly exhibits a weak sixfold structure both in its phase and amplitude, which results from the anisotropic pairing, Eq. (3.1). This behavior is similar to that of the d-wave case,[29] but sixfold symmetric here. In Fig. 2, we show a contour plot of the amplitude of $\Delta(\mathbf{r})$. The amplitude $|\Delta(\mathbf{r})|$ is slightly suppressed in the x axis direction and its equivalent directions. As shown in Fig. 2, the spatial variation of $\Delta(\mathbf{r})$ has weak anisotropy, but is almost circularly symmetric. However, the LDOS shows the characteristic sixfold symmetric structure as mentioned below.

B. Local Density of States

The LDOS calculated using the self-consistent pair potential has almost the same structure, except for the length scale for its spread, as that calculated using a test-potential $\Delta(\mathbf{r}) = \Delta(T)\tanh(r/\xi)\exp(i\phi)$ does, where $\Delta(T)$ is the uniform gap at the temperature T, $\xi = v_{\rm F0}/\Delta(T)$, and the cylindrical coordinate system $\mathbf{r} = (r, \phi)$ is taken. That is, the LDOS does not so affected by the weak sixfold symmetric spatial structure of the real-space variation part of the pair potential, $\Delta(\mathbf{r})$. We have seen the same situation also in the d-wave case.[29] It means that a calculated sixfold or fourfold structure of the LDOS directly results from the k-space variation part of the pair potential, $F(\theta)$.

In Fig. 3, we show the LDOS $N(E, \mathbf{r})$ for several energies E in the case $c_{\rm A} = 1/3$, calculated by using the self-consistently obtained pair potential. It is seen from Fig. 3(a) that the sixfold star centered at the vortex center is oriented away from the x axis by 30° for $E = 0$. Next it is seen from Fig. 3(b) that at the intermediate energy each ray splits into two parallel rays, keeping its direction. This characteristic feature was precisely observed in the experiment by Hess.[21,22] With increasing the energy E further, the sixfold star becomes a more extended one, and its orientation rotates by 30° as seen from Fig. 3(c). Note that in Fig. 3(c) the head of each ray splits in two. It coincides with an experimental result (see the STM image for 0.48 mV in Fig. 1 of Ref. 21). In this way, the anisotropic s-wave gap model well reproduces the experimental features mentioned in Sec. I: (1) the sixfold star shape, (2) the 30° rotation, and especially (3) the split parallel ray structure at the intermediate energy. We refer to Fig. 1 in Ref. 31 where the density plots of the LDOS compared with the experimental data are displayed, which is complimentary to Fig. 3 in the present paper.

Another way to examine the quasiparticle excitations in the vortex states is to see how the spectrum evolves along radial lines from the vortex center. We show the spectral evolutions along the radial lines for 30° in Fig. 4(a), 15° in 4(b), and 0° in 4(c) from the x axis. The zero-bias peak splits into several peaks in each spectral evolution. Cross sections of each spectral evolution at $r = 1$ ($r = \sqrt{x^2 + y^2}$) are shown in Fig. 5 to provide the identification of each ridge in Fig. 4.

In the calculation of Figs. 3 and 4, the smearing factor is chosen as $\eta = 0.03$, which well reproduces the STM experimental data. It corresponds to the solid lines of Fig. 5, where the peaks are labeled α–ε. The case with smaller smearing effect ($\eta = 0.001$) is represented by the dashed lines in Fig. 5, where the spectrum has the sharp peaks labeled as A–E. (The structure of these peaks is discussed in the next section.) As shown in Fig. 5, by increasing the smearing effect, the spectrum of the dashed line ($\eta = 0.001$) is reduced to that of the solid line ($\eta = 0.03$), and reproduces the STM experimental data. It seems that the LDOS actually observed in STM experiments is somewhat smeared due to impurities[16,18] or other smearing effects.[42]

In Fig. 4(a) (the 30° direction), there exist one peak at $E = 0$ and three pairs of peaks. The peak at $E = 0$ in Fig. 4(a) [the ε peak in Fig. 5(a)] corresponds to the ray which extends in the 30° direction in Fig. 3(a). This peak is referred to as the inner peak in Refs. 7 and 23. This inner peak [the ε peak] corresponds to also the split parallel ray in Fig. 3(b) and the head of the ray which splits into two in Fig. 3(c). The inner ε peak is, therefore, sensitive to the angle of the radial line, and splits in a pair of peaks with the variation of the angle [see Figs. 4(b) and 4(c)]. On the other hand, the most inside pair of peaks in Fig. 4(a) [the δ peak in Figs. 4 and 5] is not sensitive to the angle. This peak is referred to as the outer peak.[7,23] The behavior of the calculated inner and outer peaks well coincide with the experimental result (the experimental finding (4) in Sec. I). The positions of the outer δ and inner ε peaks as a function of r are compared with the experimental data in Fig. 3 of Ref. 31.

Outside the inner ε and outer δ peaks, extra peaks appear in each calculated spectral evolution [the α, β, and γ peaks in Figs. 4 and 5]. The result of the calculation shows that the extra peaks are relatively sensitive to the angle of the radial line. The existence of the extra peaks is characteristic of the gap anisotropy effect. The peaks α and β merge into the upper edge of the energy gap, $1 + c_{\rm A}$, far from the vortex. These extra peaks have not been noted in experimental data so far. While each peak cannot be clearly identified in experimental data yet, it seems that there is at least one new line outside the outer peak in the data.[50] It is expected for future experiments to definitely identify the extra peaks.

The dependence of the LDOS on the angle of the radial line is important, because it gives a detailed information on the gap anisotropy. To see it, we show in Fig. 6 a spectral evolution from the angle 0° to 30° along a circle whose radius $r = 1$. From this, we can see how each peak moves, and joins up the others with the variation of the angle. As mentioned above, the ε peak (that is, inner peak) is sensitive to the angle ϕ of the radial line, and the δ peak (outer peak) is insensitive to ϕ. The ε peak is located at $E = 0$ for $\phi = 30°$. When ϕ deviates from 30°, the peak splits into two which are positive and negative energy peaks. With decreasing ϕ to 0°, the energy E-position of the ε peak increases. As for the peaks α, β, and γ, with decreasing ϕ from 30° to 0°, the E-position decreases for the γ peak, increases for the β peak, and is insensitive for the α peak. The peaks β and γ overlap each other for $\phi = 30°$, and the peaks α and β overlap each other for $\phi = 0°$ (see also Fig. 5). Here, we should mention the behavior of the γ peak at $\phi \sim 0°$. In Fig. 6, the γ peak seems to join up the angle-insensitive δ peak near 0°, that is, the γ peak is buried in the δ peak in Figs. 4(c) and 5(c) (the 0° direction). Such a behavior of the γ peak intimately relates to the value of the anisotropic gap parameter, $c_{\rm A}$. The above behavior of γ is that of the case $c_{\rm A} = 1/3$. According as $c_{\rm A}$ increases further, the position of the γ peak at 0° shifts to the higher energy side [see a spectral evolution shown in Fig. 3(a) of Ref. 31 (the 0° direction), where $c_{\rm A}$ is set to 1/2 and we can see that a peak line, which corresponds to the present peak γ (not denoted explicitly in that figure), evolves away from the δ peak line].

IV. QUASIPARTICLE TRAJECTORIES

In this section, we interpret the behavior of the quasiparticle bounded around a vortex in terms of the quasiclassical picture.

A. Direction-dependent Local Density of States

In the quasiclassical approximation, the equations are independently given for each direction of $\bar{\mathbf{k}}$. The Eilenberger equation (or the Riccati equation) for a direction $\bar{\mathbf{k}}$ is independent of those for the other directions. The direction-dependent local density of states $N(E, \mathbf{r}, \theta)$ introduced in Eq. (2.10) is obtained from the solution of the equation for the direction $\bar{\mathbf{k}} = (\cos\theta, \sin\theta)$. The LDOS $N(E, \mathbf{r})$ is calculated by integrating the direction-dependent LDOS $N(E, \mathbf{r}, \theta)$ over θ. In an isolated vortex state, the structure of $N(E, \mathbf{r}, \theta)$ was previously investigated analytically[4,15,17] and numerically.[15] According to the results of these investigations, $N(E, \mathbf{r}, \theta)$ has the following structure for low energies below Δ_0 in the isolated single vortex.[4,15,17] (Here, remind ourselves of the notation: $\mathbf{r} = x\bar{\mathbf{x}} + y\bar{\mathbf{y}} = r_\parallel \bar{\mathbf{u}} + r_\perp \bar{\mathbf{v}}$; $\bar{\mathbf{u}} = \cos\theta\bar{\mathbf{x}} + \sin\theta\bar{\mathbf{y}}$, $\bar{\mathbf{v}} = -\sin\theta\bar{\mathbf{x}} + \cos\theta\bar{\mathbf{y}}$.) (i) $N(E, \mathbf{r}, \theta)$ as a function of $\mathbf{r} = (r_\parallel, r_\perp)$ vanishes everywhere except on a straight line along which $r_\perp = const. = r_\perp(E)$. This straight line and $r_\perp(E)$ are referred to as "quasiparticle path" and "impact parameter," respectively. (ii) Along the line $r_\perp = r_\perp(E)$, $N(E, \mathbf{r}, \theta)$ has a single maximum at $r_\parallel = 0$ and decreases exponentially for $r_\parallel \to \pm\infty$. (iii) The impact parameter $r_\perp(E)$ is a monotonically increasing function of E. One defines $E(r_\perp)$ as the energy level of the state on the quasiparticle path with the impact parameter $r_\perp$. In extreme type II superconductors where $\kappa \gg 1$, $E(r_\perp)$ is determined by the minimum value of the

amplitude of the pair potential on the quasiparticle path $r_\perp = r_\perp(E)$. For the low energy levels, $E(r_\perp)$ is given by $E(r_\perp)$=sgn$(r_\perp)|\Delta(r_\parallel = 0, r_\perp)|$ in a good approximation.

On the basis of the above properties (i)–(iii) of the direction-dependent LDOS $N(E, \mathbf{r}, \theta)$ studied by Kramer and Pesch,[4] Klein,[15] and Ullah *et al.*,[17] we interpret our result of the preceding section as follows.

For simplicity, we concentrate our attention to Eq. (2.11) as a representative. Dividing Eq. (2.11) by $F(\theta)$, we rewrite this equation as

$$\frac{1}{F(\theta)}\frac{d}{dr_\parallel}a(\omega_n, \mathbf{r}, \theta) - \Delta(\mathbf{r}) + \Big(2\frac{\omega_n}{F(\theta)} + \Delta^*(\mathbf{r})a(\omega_n, \mathbf{r}, \theta)\Big)a(\omega_n, \mathbf{r}, \theta) = 0. \qquad (4.1)$$

In the case of the isotropic s-wave pairing ($F(\theta) = 1$), $N(E, \mathbf{r}, \theta)$ at a fixed energy has the identical structure for each direction θ [the items (i), (ii), and (iii)]. Then the LDOS $N(E, \mathbf{r})$, obtained by integrating $N(E, \mathbf{r}, \theta)$ over θ, exhibits a "ring" shaped structure[24] in the real space. The impact parameter is the radius of the ring.

In the case of an anisotropic pairing, the situation is changed because of the terms which include $F(\theta)$ in Eq. (4.1). According to Eq. (4.1), both the length scale in the $r_\parallel$-direction and the energy scale vary with θ, but otherwise the form of the equation is same as that of the isotropic s-wave case. For the direction θ where $F(\theta)$ is suppressed, the length of the spreading of $N(E, \mathbf{r}, \theta)$ along the quasiparticle path [note the items (i) and (ii)] becomes large. For the same θ, the effective energy becomes large and then the impact parameter becomes far from the vortex center [note the item (iii)].

B. Interpretation on the LDOS around a vortex

We show the partly integrated $N(E, \mathbf{r}, \theta)$ in Fig. 7, where the integration is done from $\theta = -30°$ to $30°$, and its schematic figure in Fig. 8, for the pairing of Eq. (3.1) where $c_\mathrm{A} = 1/3$. Here, to clarify the structure of the LDOS, a small smearing parameter ($\eta = 0.001$) is adopted. The peak lines shown in Fig. 7 are composed of the quasiparticle paths of each direction θ described above. These peak lines can be interpreted as the flows of quasiparticles shown in Fig. 8. It is noted that the trajectories 1 and 2 appear, because $F(\theta)$ is finite at $\theta = -30°$ and $30°$, i.e., the impact parameter is finite at these angles. If $F(\theta)$ has a node, i.e., $c_\mathrm{A} = 1$, the impact parameter is infinitely far from the vortex center for the quasiparticle path of the node direction,[51] and the trajectories 1 and 2 disappear. In the bound states, the quasiparticles flow along these trajectories. We call it "quasiparticle trajectory." The whole state at a fixed energy is composed of such flows of quasiparticles along the quasiparticle trajectories, while the individual quasiparticle paths of each direction θ [the items (i) and (ii)] could be considered to be the Andreev reflections.

We show in Fig. 9 the LDOS $N(E, \mathbf{r})$ obtained by integrating the direction-dependent LDOS $N(E, \mathbf{r}, \theta)$ over all θ. A schematic figure which corresponds to Fig. 9 is shown in Fig. 10. The peaks which the radial lines cross are labeled A–E there. When the energy E elevates, the scale of the trajectory in Fig. 10 increases with keeping its structure fixed. Therefore, the trajectory has one-to-one correspondence to the peak of the spectrum of Figs. 4–6. The peaks A–E of Fig. 10 precisely correspond to those of Fig. 5. These peaks are smeared to appear as α–ε peaks in Fig. 5 (and thus in Figs. 4 and 6). The LDOS actually observed in STM experiments is not that shown in Fig. 9 itself, but somewhat smeared one [Figs. 3, 4, and 5] due to impurities[16,18] or other smearing effects.[42] Roughly speaking, the peaks A, B, C, D1, and E correspond to the peaks α, β, γ, δ, and ε, respectively.

The trajectory of Fig. 10 helps us to facilitate an understanding of the rich structure of the LDOS. The trajectories B and C cross each other at the angle $\phi = 30°$ from the x-axis in Fig. 10. Then, the peaks B and C (i.e., β and γ) overlap each other in Figs. 4(a) and 5(a). The cross of the trajectories A and B at $\phi = 0°$ in Fig. 10 corresponds to the overlap of the peaks A and B (i.e., α and β) in Figs. 4(c) and 5(c). When ϕ varies from $30°$ to $0°$, the trajectories C and D1 cross each other in Fig. 10, where $c_\mathrm{A} = 1/3$. It corresponds to the result that the peaks γ and δ interchange their positions between Figs. 5(b) and 5(c). However, this behavior of γ and δ depends on the anisotropic gap parameter c_A as mentioned at the end of Sec. III. In the case of large c_A, the trajectories C and D1 does not cross for $0° \le \phi \le 30°$ in Fig. 10. Even at $\phi = 0°$, the trajectory D1 is located farther from the vortex center than the trajectory C, for large c_A. Then, the peak C (i.e., γ) is located at higher energy than the peak D1 (i.e., δ) in the spectrum of Figs. 5(c) and 6, for large c_A. As seen in Fig. 5, the peak D2 tends to be buried in the other peaks, due to the smearing effects. However, if the experiment is performed for the weak smearing case, the peak D2 should be observed as a small peak, which splits from the peak D1 (i.e., δ) at $\phi = 30°$ and approaches the peak E (i.e., ε) with decreasing ϕ to $0°$. This D2 peak seems to be easily observed for the angle $0° < \phi < 10°$. We detect a small indication of the D2 peak for this angle region, if Fig. 6 is enlarged at $\phi \sim 0°$. The trajectories D1 and E (i.e., δ and ε) corresponds to the trajectories 1 and 2 of Fig. 8, which is related to the lower edge of the anisotropic energy gap. Therefore, these trajectories disappear for the higher energy, $(1 - c_\mathrm{A}) < E < (1 + c_\mathrm{A})$. The peaks D1 and E (i.e., δ and ε) merge into the lower edge of the energy gap at $E = 1 - c_\mathrm{A}$ far from the vortex.

C. Flows of quasiparticles around a vortex

The flows of the quasiparticles mentioned above are quantitatively represented by the following quantity,

$$\mathbf{I}(E,\mathbf{r}) = \int_0^{2\pi} \frac{d\theta}{2\pi} \rho(\theta)\mathbf{v}_{\rm F}(\theta) N(E,\mathbf{r},\theta), \tag{4.2}$$

which we tentatively call "directional local density of states." This directional LDOS corresponds to a quantity obtained by integrating "spectral current density" introduced by Rainer *et al.*[39] over θ (or $\mathbf{p}_f$ in Ref. 39). The total current density around a vortex is composed of the spectral current density.[39] In Figs. 11(a), 11(b), 11(c), and 11(d), we show the directional LDOS $\mathbf{I}(E,\mathbf{r})$ calculated for $E = 0.2$, 1.2, 1.4, and 1.6, respectively. Here $\mathbf{I}(E,\mathbf{r})$ is calculated under the condition considered in this section, i.e., under the anisotropic gap and the isotropic cylindrical Fermi surface. It is seen from Fig. 11(a) that the flow of the quasiparticle exhibits a sixfold anisotropy resulting from the sixfold LDOS of the bound states (Fig. 3(b) and thus Fig. 10). Now, it is of interest to note the flow with an energy near the upper gap edge, $E = 1+c_{\rm A}$ ($\simeq 1.3$). Comparing Figs. 11(b) and 11(d), we can see that the quasiparticles above and below the upper gap edge flow each other in reverse directions except in the vicinity of the vortex center. It certainly coincides with a result of an analysis based on the Bogoliubov-de Gennes (BdG) equation.[14] This feature should not be influenced by the gap anisotropy.

V. SUMMARY AND DISCUSSIONS

The LDOS around an isolated single vortex is studied within the framework of the quasiclassical theory. We consider the effect of the anisotropy of the superconducting energy gap. Assuming the anisotropic s-wave energy gap in Eq. (3.1), we succeed in theoretically reproducing the characteristic structure of the LDOS observed in STM experiments; the observed features, i.e., the items (1)–(4) for $NbSe_2$ listed in Sec. I, are well described in terms of the anisotropic gap model. We point out the existence of the missing peaks (α, β, and γ) at the higher energy side in the spectral evolution shown in Figs. 4–6, which is expected to be looked for in a future experiment. We also notice the further splitting of the observed broad peaks as shown, for example, in Fig. 5(b) ($\delta \rightarrow$ D1 and D2). These predictions, which reflect the gap anisotropy, may be checked by using a purer sample at lower temperatures, because smearing effects, due to lattice defects or thermal broadening, mask the fine details. We attempt to interpret the calculated LDOS in terms of the quasiparticle trajectory. This enables us to thoroughly understand the STM results and the internal electronic structure of the vortex. In this paper, the value of our parameter is chosen appropriate for $NbSe_2$. However, the essence of the obtained results should be applicable to other type II superconductors in general although the degree of the gap anisotropy $c_{\rm A}$ and the symmetry of $F(\theta)$ will be different in each case. Even in other anisotropic superconductors, the explanation in terms of the quasiparticle trajectory would be helpful to an understanding of the internal electronic structure of vortices.

A. Comparison with other theories and effects of the vortex lattice

Let us comment on prior works which are connected with the star-shaped LDOS observed in $NbSe_2$. On the basis of a sixfold perturbation, Gygi and Schlüter[20] explained that the lower and higher energy stars observed by STM were interpreted as bonding or antibonding states. The STM results (1) and (2) listed in Sec. I were able to be explained by this perturbation scheme. They adopted a sixfold crystal lattice potential in $NbSe_2$ as the perturbation. Recently, Zhu, Zhang, and Sigrist[52] investigated the effect of the underlying crystal lattice by means of a non-perturbation method, i.e., a method of diagonalizing a tight-binding BdG Hamiltonian in a discrete square lattice, where the crystal lattice potential, i.e., the band structure is determined a priori. This method supplements the perturbation theory of Ref. 20: the absolute orientation of the star relative to the underlying crystal lattice was determined.[52]

By this non-perturbation approach, also a gradual rotation of the star-shaped LDOS was obtained in the intermediate energy region.[52] Nevertheless, it is not yet clear whether the crystal lattice effect is able to reproduce the remaining experimental findings (3) and (4), i.e., the split parallel ray structure and the behavior of peaks in the spectral evolutions. The model used in Ref. 52 is the discrete lattice model, and therefore it is impossible to obtain detailed spectra, e.g., spectral evolutions along radial lines, due to the discreteness. Hence, it is desired to treat the crystal lattice potential effect with a non-perturbation method in the continuum limit.

Now, the crystal lattice potential determines the band structure, and influences the structure of the Fermi surface. The effect of the crystal lattice potential should appear as the anisotropy of the Fermi surface. In our framework, the anisotropy of the Fermi surface is taken into account by assuming an anisotropic density of states at the Fermi surface, $\rho(\theta)$, which appears in the θ-integral of Eq. (2.10), and the anisotropic Fermi velocity $v_{\rm F}(\theta)$, which appears in the Eilenberger (or Riccati) equations. The experimental findings (1)–(4) can be reproduced qualitatively, if we introduce a large anisotropy in $v_{\rm F}(\theta)$. Its details and the comparison of them to the present results from the gap anisotropy effect are discussed elsewhere.[33]

Gygi and Schlüter considered also the effect of nearest-neighbor vortices, i.e, that of the vortex lattice.[20] They adopted a sixfold anisotropy of the vector potential as the vortex lattice effect, and treated it as the perturbation. However, the periodicity of the pair potential is also important as the effect of the vortex lattice.[15,18] In extreme type II superconductors such as $NbSe_2$ where $\kappa \gg 1$, the periodicity of the pair potential is expected to have

stronger effects upon the structure of the LDOS than the anisotropy of the vector potential does. We find in Ref. 32 that the effect of the periodicity gives a characteristic sixfold structure to the LDOS.

This structure of the LDOS which results from the periodicity of the pair potential appears only at high magnetic fields such as 1 T for the material parameters appropriate to $NbSe_2$, where the vortex core regions substantially overlap each other.[32] At a lower magnetic field such as 0.1 T, the calculated LDOS reduces to the almost circular structure. On the other hand, the LDOS observed in a STM experiment exhibits the star-shaped structure in spite of a low field 0.025 T (see Fig. 12 in Ref. 53). Therefore, in the case of $NbSe_2$ at low magnetic fields, we need to consider the effects of anisotropy other than the vortex lattice effect in order to explain the star-shaped LDOS. Both the vortex lattice effect and the anisotropic superconducting gap one are important for the star-shaped LDOS observed in $NbSe_2$ at high magnetic fields. We expect a future STM experiment to be performed on isotropic superconducting compounds or metals to clarify the vortex lattice effect and confirm predictions of Ref. 32.

In STM experiments on $NbSe_2$, one of the directions of nearest-neighbor vortices coincides with the a axis (see the literature by Hess *et al.*[7,8,19,21–23,53,54] or Renner *et al.*[9]), except for extreme low fields.[55] This experimental fact gives evidence of a correlation of the vortex lattice with the underlying crystal lattice of $NbSe_2$. It was recently found that in d-wave superconductors, higher-order (nonlocal correction) terms in the Ginzburg-Landau equation, which reflect the fourfold symmetric property of the d-wave pairing, give rise to a preferred direction of the vortex lattice.[56,57] In $NbSe_2$, the sixfold anisotropic pairing, Eq. (3.1), is expected to give rise to the same correlation as the d-wave pairing does, and it may be the origin of the experimental fact mentioned above. A possibility of the correlation of the vortex lattice with the underlying crystal lattice was recently reported also in a high T_c cuprate.[58,59]

B. Beyond the quasiclassical approach

We mention the LDOS around a vortex in high T_c cuprates. It seems from various experiments that high T_c material is a d-wave superconductor.[60] A fourfold structure of the LDOS is predicted in d-wave superconductors by theoretical studies based on the quasiclassical theory.[24,25,29] The origin of this fourfold structure is same as that discussed in the present paper for the gap anisotropy. Recently, Maggio-Aprile *et al.* observed tunneling spectra around vortices in a high T_c cuprate, $YBa_2Cu_3O_{7-\delta}$, with STM.[61,62,59] However, the spectroscopic images of STM have not exhibited any sign of a fourfold structure yet. We expect further detailed experiments to observe the fourfold symmetric LDOS structure.

When we consider the high T_c materials, the quantum effects should be taken into account. The quasiclassical theory is certainly valid only in systems where the atomic scale spatial variation of the Green's function can be neglected with respect to the coherence length scale one.[28,63] The effects neglected in the quasiclassical theory can be important in the case of the high T_c cuprate; the quantization of energy levels of the bound states cannot be treated by the quasiclassical theory, and while it is possible in the quasiclassical approximation to divide the equation into individual equations for each direction of $\bar{\mathbf{k}}$, it is impossible in the quantum-mechanical limit. Although we expect the fourfold structure of the LDOS should be observed in future experiments, the above effects may change the situation in the case of the high T_c cuprate. It is certainly desired on the theoretical side that a fully quantum-mechanical approach clears up this problem in future.

As for the fully quantum-mechanical approach, it is needed to solve the BdG equation without quasiclassical approximations. The BdG equation cannot be written in a local form in the case of an anisotropic pairing, and therefore it is difficult to treat this equation in the continuum limit. One of the possible approaches to this problem is the method of diagonalizing a BdG Hamiltonian for a specific lattice model.[52,64–67] In the lattice model, however, the atomic scale variation of wave functions among the lattice points is uncertain.

In most superconductors ($\xi \gg 1/k_{\mathrm{F}}$), the atomic scale variation of the wave function is a redundant information and can usually be neglected on the basis of the quasiclassical theory. On the other hand, in the high T_c cuprate superconductors, $k_{\mathrm{F}}\xi \simeq \varepsilon_{\mathrm{F}}/\Delta_0 \sim 1$ (the Fermi wave-number and energy are k_{F} and ε_{F}, respectively),[63] and therefore the atomic scale variation and the quantization of bound states in a vortex may be crucial for the electronic structure around the vortex in the cuprates.

The high T_c cuprate is certainly the only superconductor possessed of a possibility of an experimentally detectable quantization in the vortex bound states. According to Ref. 1, a substantial energy quantization (of the order of $\Delta_0^2/\varepsilon_{\mathrm{F}} \sim 10$ K) is expected to exist in the high T_c cuprate. However, to the present author's knowledge, the system considered in Ref. 1 is an isotropic s-wave superconductor and the mechanism of the quantization in the case of anisotropic pairing is not yet understood. In case of gap node due to anisotropic pairing, it is expected that the separation of the energy levels becomes small. Further experiments, which, e.g., investigate spatial variation of this quantized bound states in the high T_c cuprates with STM and then compare its result with the quasiclassical prediction[24,25,29] in order to clarify how the quantum effects mentioned above modify the vortex bound states, are the need for alternative theoretical studies of the vortex bound states.

C. Concluding remarks

The electronic structure of vortices in a compound, $LuNi_2B_2C$, was quite recently investigated by STM.[68,69] Although no conductance peaks related to localized quasiparticle states in the vortex core are observed in the experiment, due to a short mean free path (of the order of the coherence length) and thermal broadening effects at 4.2 K ($T_c \approx 16\ K$),[68] a rich (maybe fourfold) structure of the LDOS such as that discussed in the present paper is expected to be detected in STM spectra by lowering the temperature and decreasing impurities or defects. If an anisotropic bound states around a single vortex is observed, it should suggest an anisotropy of the pairing in this compound. The direction (in the k-space) in which the superconducting gap is suppressed corresponds to that (in the real space) of a ray of the LDOS at zero bias.

Finally, low-temperature STM is the unique experimental method which has the ability not only to image the distribution of the vortex lattice, but also to probe the electronic structure of individual vortices. We expect future STM experiments to be performed in vortex states on various superconductors such as organic conductors, high T_c cuprates, heavy Fermion superconductors (e.g., UPt_3), and a recently discovered non-copper-layered perovskite superconductor, Sr_2RuO_4[70] which has nearly cylindrical Fermi surfaces[71,72] and a possibility that an odd-parity superconductivity would be realized in it.[73,74] The information on the vortex bound states available from STM spectra can be one of clues to the pairing. The low-temperature STM experiments deserve a great deal of attention.

ACKNOWLEDGMENTS

It is our pleasure to thank H. F. Hess for fruitful suggestion on the present issue, useful communication of results, and helpful discussions. We are also grateful to N. Schopohl for sending useful information on the Riccati equation and to Ch. Renner for useful discussion of their experiments. We are indebted to the Supercomputer Center of the Institute for Solid State Physics, University of Tokyo, for part of the numerical calculations. One of us (M.I.) is supported by the Japan Society for the Promotion of Science for Young Scientists.

[1] C. Caroli, P. G. de Gennes, and J. Matricon, Phys. Lett. **9**, 307 (1964).
[2] R. Leadon and H. Suhl, Phys. Rev. **165**, 596 (1968).
[3] J. Bardeen, R. Kümmel, A. E. Jacobs, and L. Tewordt, Phys. Rev. **187**, 556 (1969).
[4] L. Kramer and W. Pesch, Z. Phys. **269**, 59 (1974).
[5] R. J. Watts-Tobin, L. Kramer, and W. Pesch, J. Low Temp. Phys. **17**, 71 (1974).
[6] See for a comprehensive review article, A. Khurana, Phys. Today **43**, No. 6, 17 (1990).
[7] H. F. Hess, in *Scanning Tunneling Microscopy*, edited by J. A. Stroscio and W. J. Kaiser (Academic Press, San Diego, 1993), p. 427.
[8] H. F. Hess, R. B. Robinson, R. C. Dynes, J. M. Valles, Jr., and J. V. Waszczak, Phys. Rev. Lett. **62**, 214 (1989).
[9] Ch. Renner, A. D. Kent, Ph. Niedermann, Ø. Fischer, and F. Lévy, Phys. Rev. Lett. **67**, 1650 (1991).
[10] A. W. Overhauser and L. L. Daemen, Phys. Rev. Lett. **62**, 1691 (1989).
[11] L. L. Daemen and A. W. Overhauser, Phys. Rev. B **40**, 10778 (1989).
[12] J. D. Shore, M. Huang, A. T. Dorsey, and J. P. Sethna, Phys. Rev. Lett. **62**, 3089 (1989).
[13] F. Gygi and M. Schlüter, Phys. Rev. B **41**, 822 (1990).
[14] F. Gygi and M. Schlüter, Phys. Rev. B **43**, 7609 (1991).
[15] U. Klein, Phys. Rev. B **40**, 6601 (1989).
[16] U. Klein, Phys. Rev. B **41**, 4819 (1990).
[17] S. Ullah, A. T. Dorsey, and L. J. Buchholtz, Phys. Rev. B **42**, 9950 (1990).
[18] B. Pöttinger and U. Klein, Phys. Rev. Lett. **70**, 2806 (1993).
[19] H. F. Hess, R. B. Robinson, and J. V. Waszczak, Phys. Rev. Lett. **64**, 2711 (1990).
[20] F. Gygi and M. Schlüter, Phys. Rev. Lett. **65**, 1820 (1990). See also Sec. IV of Ref. 14.
[21] H. F. Hess, Physica C **185-189**, 259 (1991).
[22] H. F. Hess, Jpn. J. Appl. Phys. Series **9**, 270 (1993).
[23] H. F. Hess, R. B. Robinson, and J. V. Waszczak, Physica B **169**, 422 (1991).
[24] N. Schopohl and K. Maki, Phys. Rev. B **52**, 490 (1995).
[25] K. Maki, N. Schopohl, and H. Won, Physica B **204**, 214 (1995).
[26] G. Eilenberger, Z. Phys. **214**, 195 (1968).
[27] A. I. Larkin and Yu. N. Ovchinnikov, Zh. Eksp. Teor. Fiz. **55**, 2262 (1968) [Sov. Phys. JETP **28**, 1200 (1969)].
[28] See for a review article of the quasiclassical theory, J. W. Serene and D. Rainer, Phys. Rep. **101**, 221 (1983).
[29] M. Ichioka, N. Hayashi, N. Enomoto, and K. Machida, Phys. Rev. B **53**, 15316 (1996).
[30] The present authors are greatly indebted to H. F. Hess for bringing this similarity to their attention.
[31] N. Hayashi, M. Ichioka, and K. Machida, Phys. Rev. Lett. **77**, 4074 (1996).
[32] M. Ichioka, N. Hayashi, and K. Machida, Phys. Rev. B. **55**, 6565 (1997).
[33] N. Hayashi, M. Ichioka, and K. Machida, in preparation.
[34] See for the Fermi surface of $NbSe_2$, R. Corcoran, P. Meeson, Y. Onuki, P. A. Probst, M. Springford, K. Takita, H. Harima, G. Y. Guo, and B. L. Gyorffy, J. Phys. Condens. Matter **6**, 4479 (1994).
[35] In three dimensional systems with a general pairing, it is needed to take account of a phase-sensitively tunneling process when we consider STM results. See Y. Tanaka and S. Kashiwaya, Phys. Rev. Lett. **74**, 3451 (1995).
[36] M. Matsumoto and H. Shiba, J. Phys. Soc. Jpn. **64**, 3384

(1995); **64**, 4867 (1995); **65**, 2194 (1996).
[37] L. J. Buchholtz, M. Palumbo, D. Rainer, and J. A. Sauls, J. Low Tmp. Phys. **101**, 1079 (1995); **101**, 1099 (1995).
[38] M. Ichioka, N. Hayashi, N. Enomoto, and K. Machida, J. Phys. Soc. Jpn. **64**, 4547 (1995); M. Ichioka, N. Enomoto, N. Hayashi, and K. Machida, Phys. Rev. B **53**, 2233 (1996); K. Machida, M. Ichioka, N. Hayashi, and N. Enomoto, Physica C **263**, 428 (1996).
[39] D. Rainer, J. A. Sauls, and D. Waxman, Phys. Rev. B **54**, 10094 (1996).
[40] U. Klein, J. Low Temp. Phys. **69**, 1 (1987).
[41] E. V. Thuneberg, J. Kurkijärvi, and D. Rainer, Phys. Rev. B **29**, 3913 (1984).
[42] R. C. Dynes, V. Narayanamurti, and J. P. Garno, Phys. Rev. Lett. **41**, 1509 (1978).
[43] N. Schopohl (unpublished).
[44] For example, W. H. Press, S. A. Teukolsky, W. T. Vetterling, and B. P. Flannery, *Numerical Recipes in FORTRAN* (Cambridge University Press, London, 1992), 2nd ed., p. 708.
[45] D. Markowitz and L. P. Kadanoff, Phys. Rev. **131**, 563 (1963).
[46] J. R. Clem, Phys. Rev. **148**, 392 (1966).
[47] J. R. Clem, Ann. Phys. (N.Y.) **40**, 268 (1966).
[48] K. Ishida, Y. Niino, G. Q. Zheng, Y. Kitaoka, K. Asayama, and T. Ohtani, J. Phys. Soc. Jpn. **65**, 2341 (1996).
[49] L. C. Hebel, Phys. Rev. **116**, 79 (1959).
[50] H. F. Hess (private communication).
[51] Strictly speaking, the states for θ in the vicinity of nodes are in the scattering state, and $N(E, \mathbf{r}, \theta)$ is spread on the real space for these θ.
[52] Y. D. Zhu, F. C. Zhang, and M. Sigrist, Phys. Rev. B **51**, 1105 (1995).
[53] H. F. Hess, C. A. Murray, and J. V. Waszczak, Phys. Rev. B **50**, 16528 (1994).
[54] H. F. Hess, C. A. Murray, and J. V. Waszczak, Phys. Rev. Lett. **69**, 2138 (1992).
[55] C. A. Bolle, F. De La Cruz, P. L. Gammel, J. V. Waszczak, and D. J. Bishop, Phys. Rev. Lett. **71**, 4039 (1993).
[56] H. Won and K. Maki, Europhys. Lett. **30**, 421 (1995); Phys. Rev. B **53**, 5927 (1996).
[57] N. Enomoto, M. Ichioka, and K. Machida, J. Phys. Soc. Jpn. **66**, 204 (1997); M. Ichioka, N. Enomoto, and K. Machida, preprint.
[58] B. Keimer, W. Y. Shih, R. W. Erwin, J. W. Lynn, F. Dogan, and I. A. Aksay, Phys. Rev. Lett. **73**, 3459 (1994).
[59] Ch. Renner, I. Maggio-Aprile, A. Erb, E. Walker, and Ø. Fischer, in *Spectroscopic Studies of Superconductors*, edited by I. Bozovic and D. van der Marel, Proc. SPIE **2696B**, 322 (1996).
[60] For example, C. C. Tsuei, J. R. Kirtley, C. C. Chi, L. S. Yu-Jahnes, A. Gupta, T. Shaw, J. Z. Sun, and M. B. Ketchen, Phys. Rev. Lett. **73**, 593 (1994).
[61] I. Maggio-Aprile, Ch. Renner, A. Erb, E. Walker, and Ø. Fischer, Phys. Rev. Lett. **75**, 2754 (1995).
[62] See for a comprehensive review article, B. G. Levi, Phys. Today **48**, No. 11, 19 (1995).
[63] Y. Morita, M. Kohmoto, and K. Maki (unpublished).
[64] P. I. Soininen, C. Kallin, and A. J. Berlinsky, Phys. Rev. B **50**, 13883 (1994).
[65] Y. Wang and A. H. MacDonald, Phys. Rev. B **52**, 3876 (1995).
[66] In lattice models, it is natural to consider an (extended) s-wave pairing in addition to the d-wave one even when on-site (s-wave pairing) interaction is repulsive. See for articles on the induced s-wave component of the pair potential around a vortex in d-wave superconductors, D. L. Feder and C. Kallin, Phys. Rev. B **55**, 559 (1997), and references therein.
[67] A calculation for the electronic structure around vortices in a d-wave superconductor was recently performed on a t-J model, where a relation between an induced s-wave component of the pair potential and the vortex bound states was investigated. A. Himeda, M. Ogata, Y. Tanaka, S. Kashiwaya, in preparation.
[68] Y. De Wilde, M. Iavarone, U. Welp, V. Metlushko, A. E. Koshelev, I. Aranson, G. W. Crabtree, and P. C. Canfield, preprint.
[69] Y. De Wilde, M. Iavarone, U. Welp, V. Metlushko, A. E. Koshelev, I. Aranson, G. W. Crabtree, P. L. Gammel, D. J. Bishop, and P. C. Canfield, preprint.
[70] Y. Maeno, H. Hashimoto, K. Yoshida, S. Nishizaki, T. Fujita, J. G. Bednorz, and F. Lichtenberg, Nature **372**, 532 (1994).
[71] T. Oguchi, Phys. Rev. B **51**, 1385 (1995).
[72] D. J. Singh, Phys. Rev. B **52**, 1358 (1995).
[73] M. Sigrist and M. E. Zhitomirsky, J. Phys. Soc. Jpn. **65**, 3452 (1996).
[74] K. Machida, M. Ozaki, and T. Ohmi, J. Phys. Soc. Jpn. **65**, 3720 (1996).

FIG. 1. The density of states $N(E)$ at zero field, where smearing parameter $\eta = 0.03$ (solid line) or $\eta = 0.001$ (dashed line). It is calculated for the isotropic cylindrical Fermi surface, and the degree of the gap anisotropy is $c_{\rm A} = 1/3$.

FIG. 2. Contour plot of the amplitude of the real-space variation part of the pair potential, $|\Delta(\mathbf{r})|$. From the center, 0.1, 0.2, ..., 0.9. The temperature is $T = 0.1T_c$, and the degree of the gap anisotropy is $c_{\rm A} = 1/3$.

FIG. 3. The LDOS $N(E, \mathbf{r})$ ($\eta = 0.03$) calculated for the energies $E = 0$ (a), 0.2 (b), and 0.4 (c). Large peaks in the vicinity of the vortex center are truncated in the figures (a) and (b).

FIG. 4. Spectral evolutions $N(E, \mathbf{r})$ ($\eta = 0.03$) along radial lines for 30° (a), 15° (b), and 0° (c) from the x axis. The zero-bias peak is truncated in the figures. The peak lines in the spectra are labeled α–ε.

FIG. 5. Cross sections of the spectral evolutions (Fig. 4) at the distance from the vortex center, $r = 1$. The directions of each radial line are 30° (a), 15° (b), and 0° (c) from the x axis. The peaks in the spectra are labeled A–E for the dashed line spectra ($\eta = 0.001$) and α–ε for the solid line spectra ($\eta = 0.03$). The labels α–ε correspond to those of Fig. 4.

FIG. 6. Spectral evolution $N(E, \mathbf{r})$ ($\eta = 0.03$) from the angle 0° to 30° along a circle whose radius $r = 1$. The center of this circle is situated at the vertex center. The peaks labeled as α–ε correspond to those of Figs. 4 and 5.

FIG. 7. The direction-dependent LDOS $N(E, \mathbf{r}, \theta)$ partly integrated from $\theta = -30°$ to 30°, where $E = 0.5$, $\eta = 0.001$, and $6\xi_0 \times 6\xi_0$ is shown in the real space.

FIG. 8. Schematic flow trajectories of quasiparticles with an energy $0 < E < (1 - c_{\rm A})$. These trajectories correspond to those shown in Fig. 7. When $(1 - c_{\rm A}) < E < (1 + c_{\rm A})$, the trajectories 1 and 2 disappear and only the trajectory 3 is alive.

FIG. 9. The LDOS $N(E, \mathbf{r})$ which is obtained by integrating the direction-dependent LDOS $N(E, \mathbf{r}, \theta)$ over θ, where $E = 0.5$, $\eta = 0.001$, and $6\xi_0 \times 6\xi_0$ is shown.

FIG. 10. Schematic figure of the LDOS $N(E, \mathbf{r})$ for an energy $0 < E < (1 - c_{\rm A})$. Points A–E correspond to the peaks of the dashed line spectra in Fig. 5.

FIG. 11. The directional LDOS $\mathbf{I}(E, \mathbf{r})$ ($\eta = 0.03$) for the energies $E = 0.2$ (a), 1.2 (b), 1.4 (c), and 1.6 (d). The arrows in the figures represent only the directions of $\mathbf{I}(E, \mathbf{r})$.

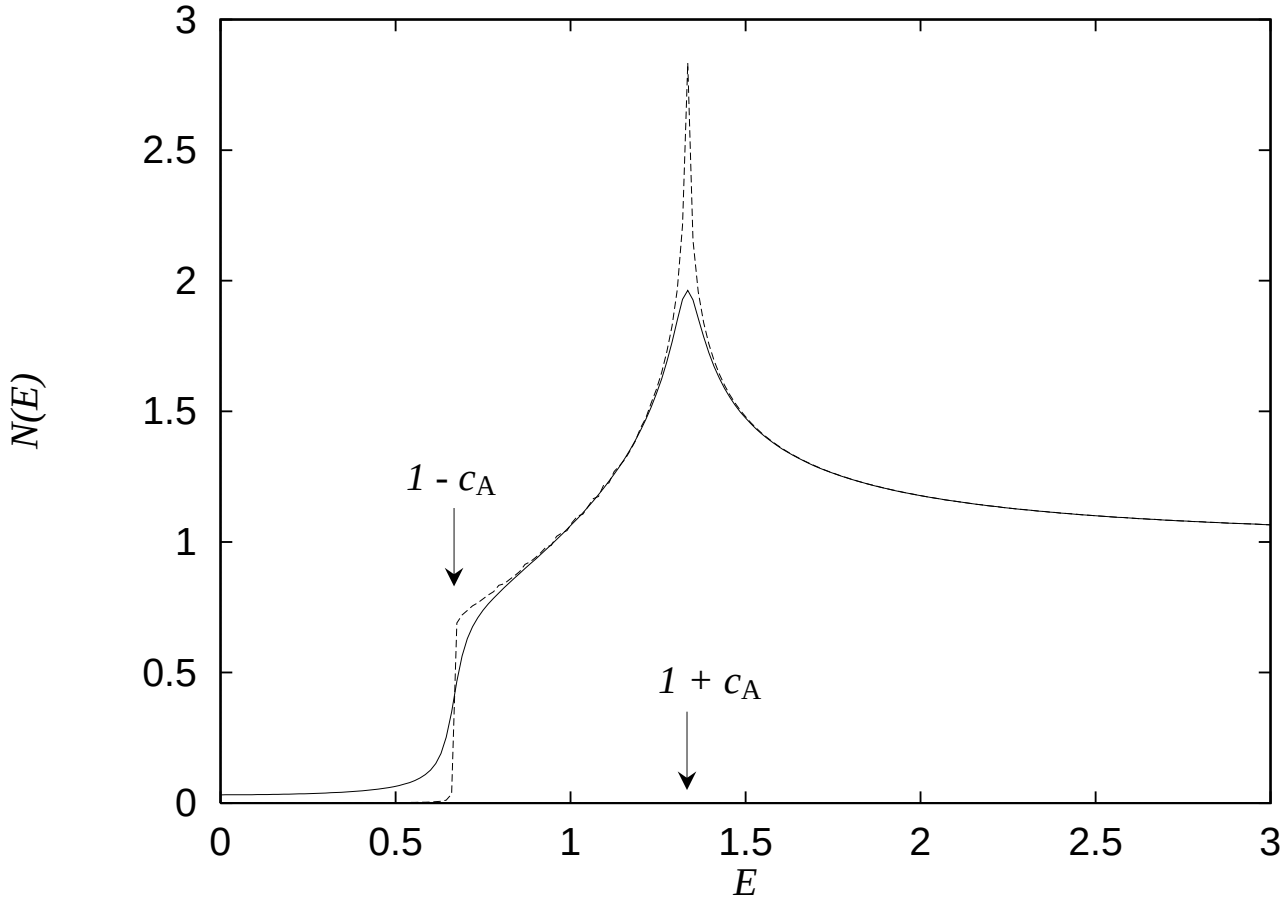

Fig. 1

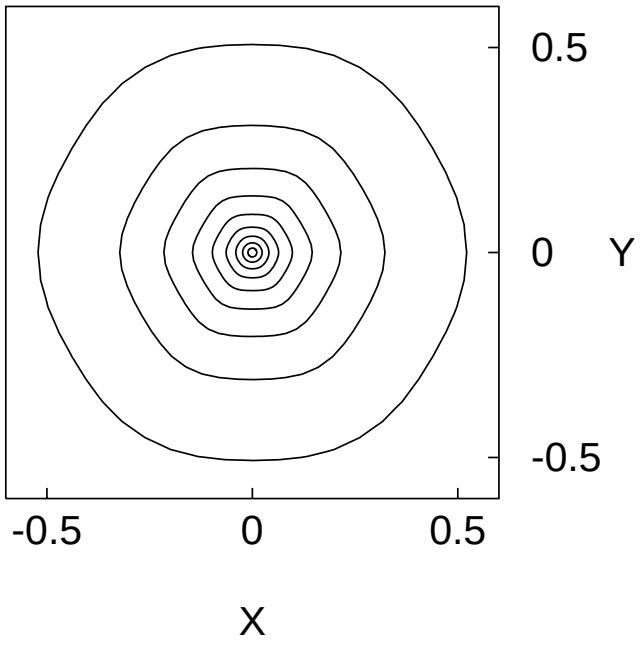

Fig. 2

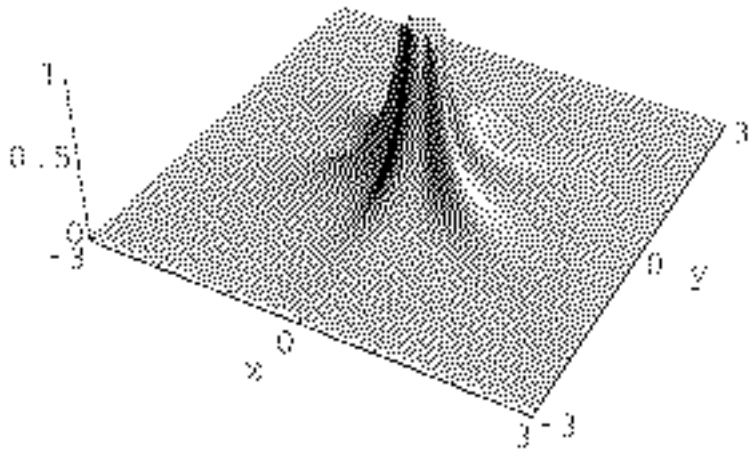

Fig. 3(a)

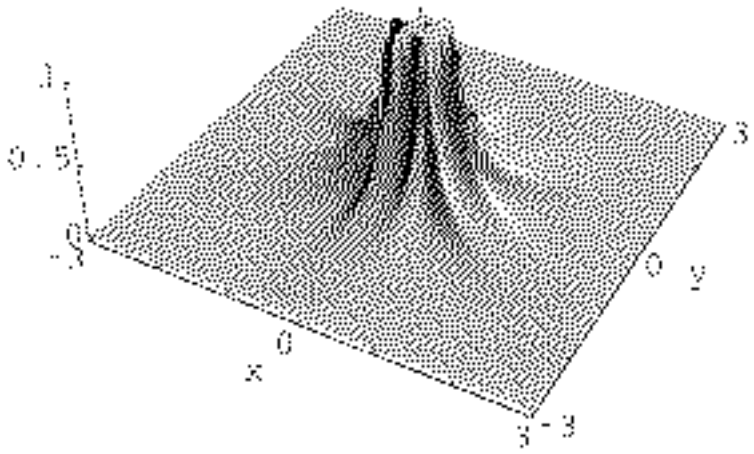

Fig. 3(b)

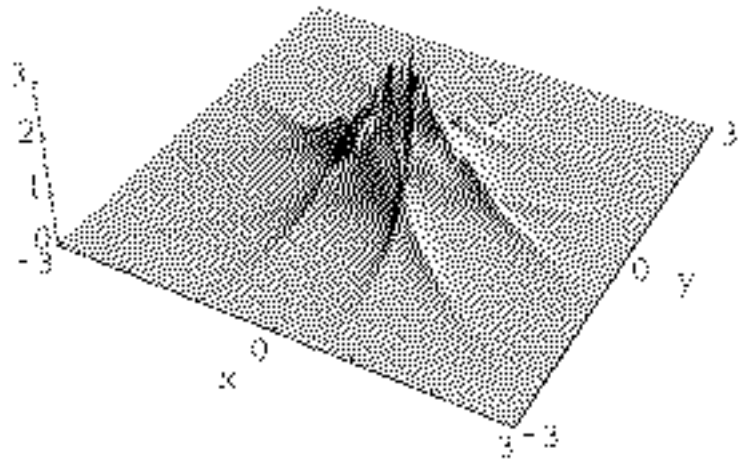

Fig. 3(c)

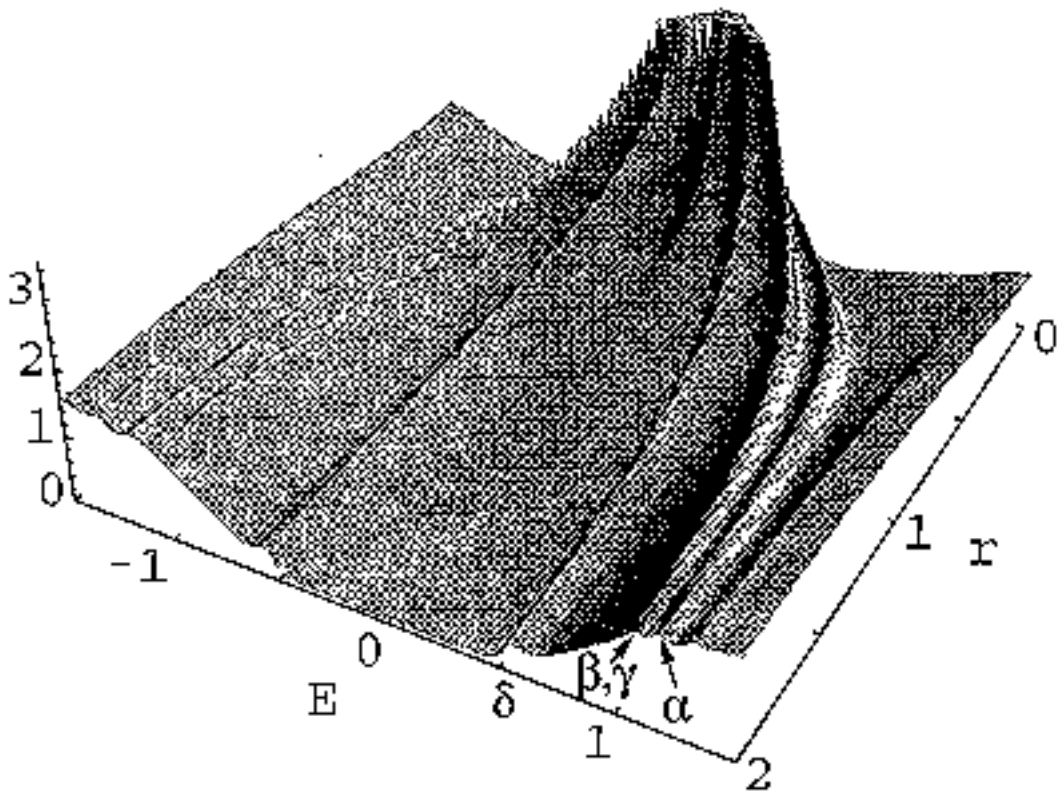

Fig. 4 (a)

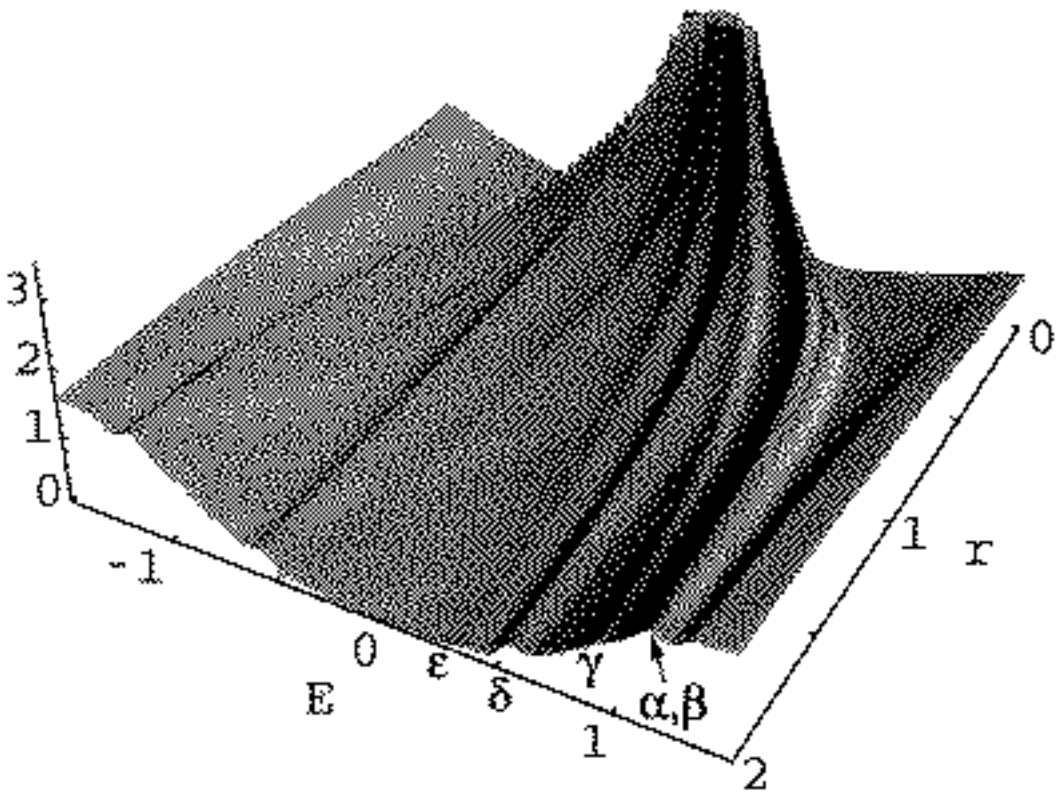

Fig. 4 (b)

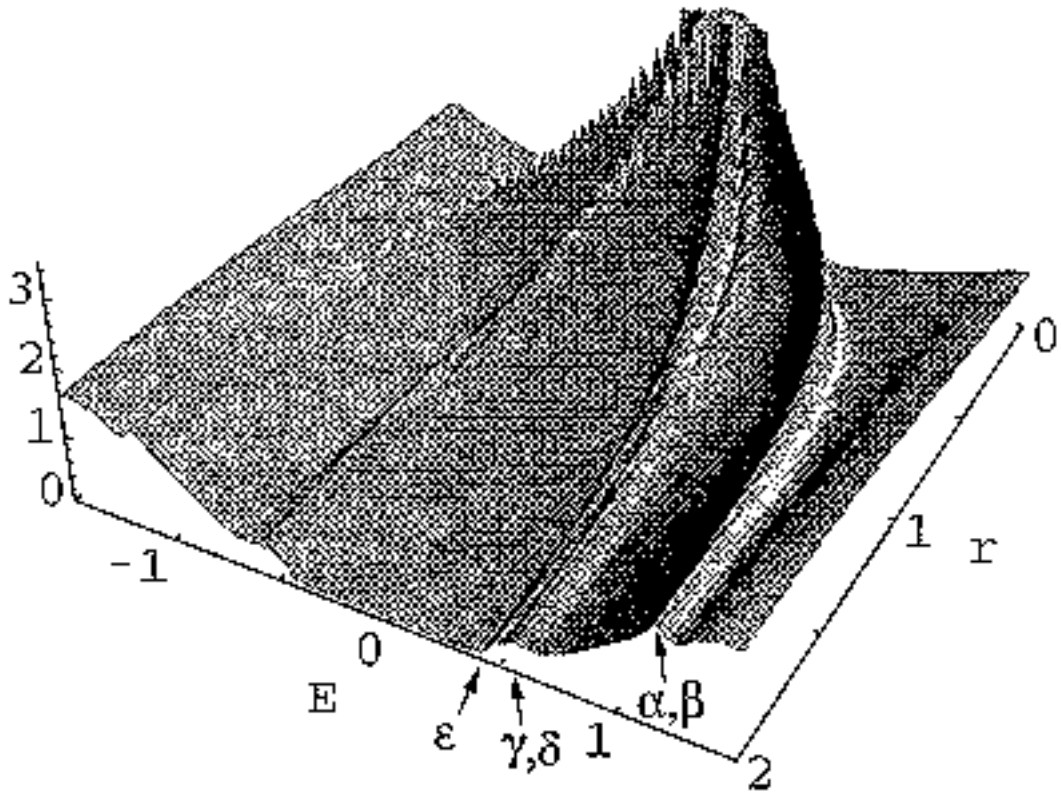

Fig. 4 (c)

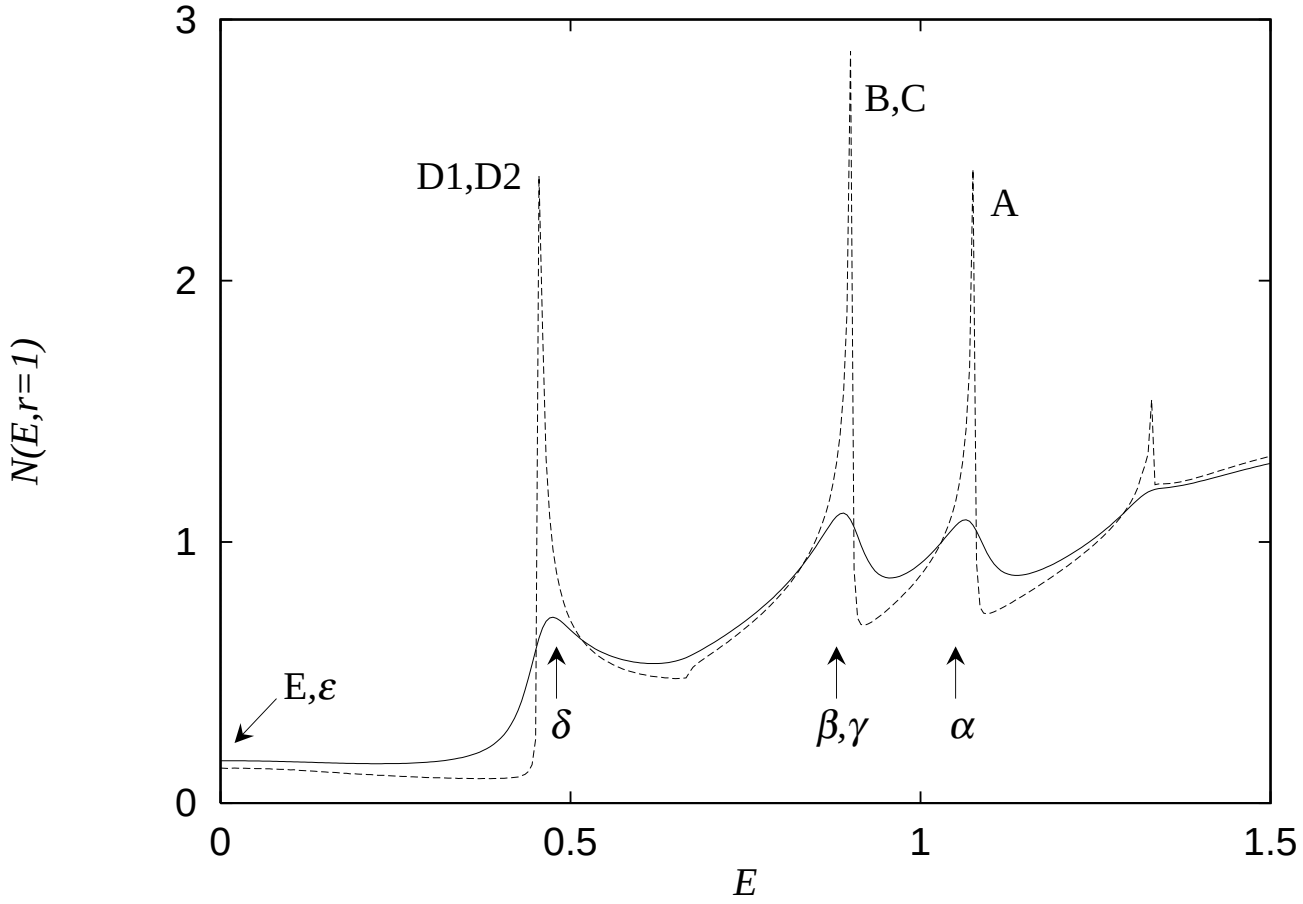

Fig. 5(a)

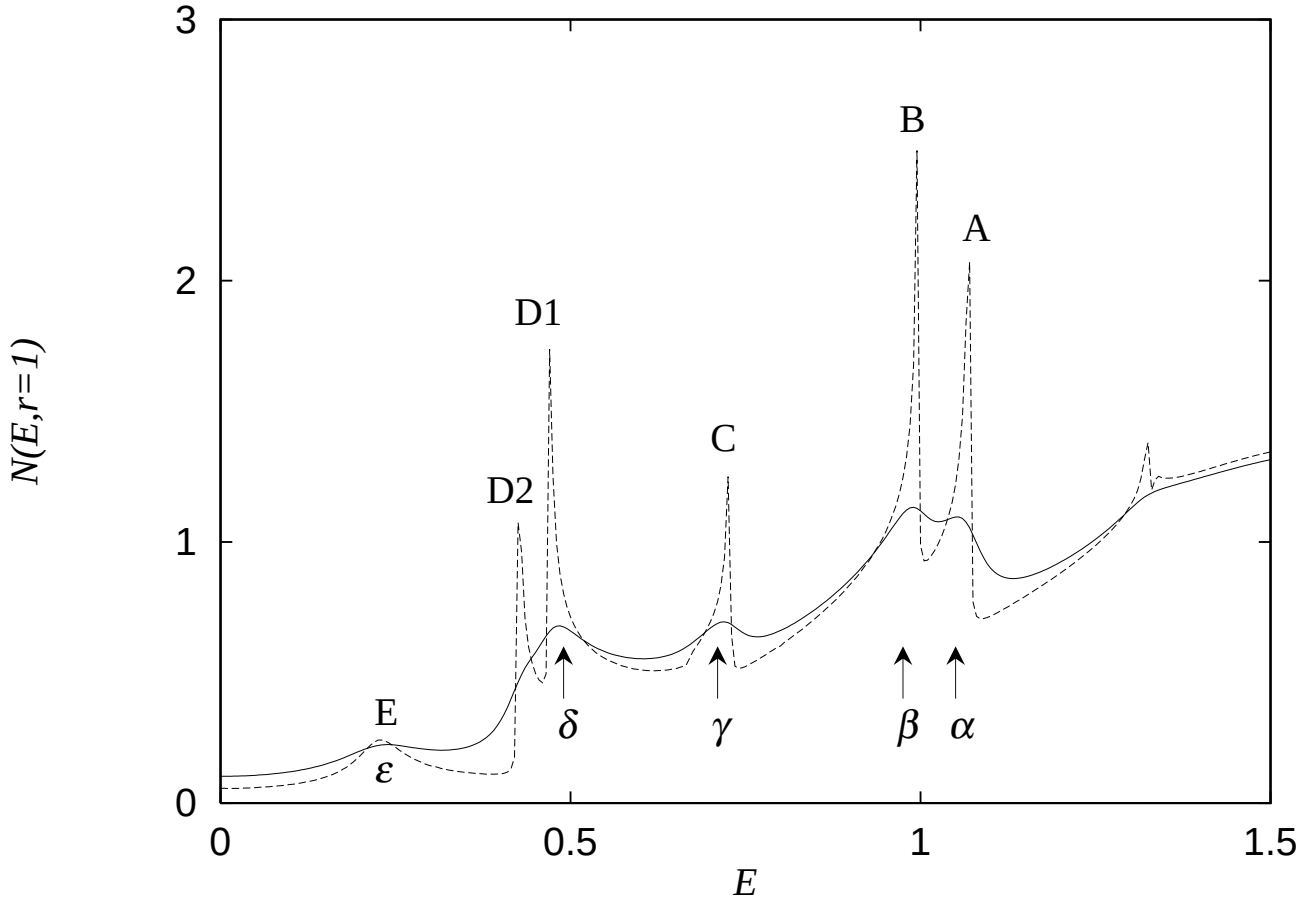

Fig. 5(b)

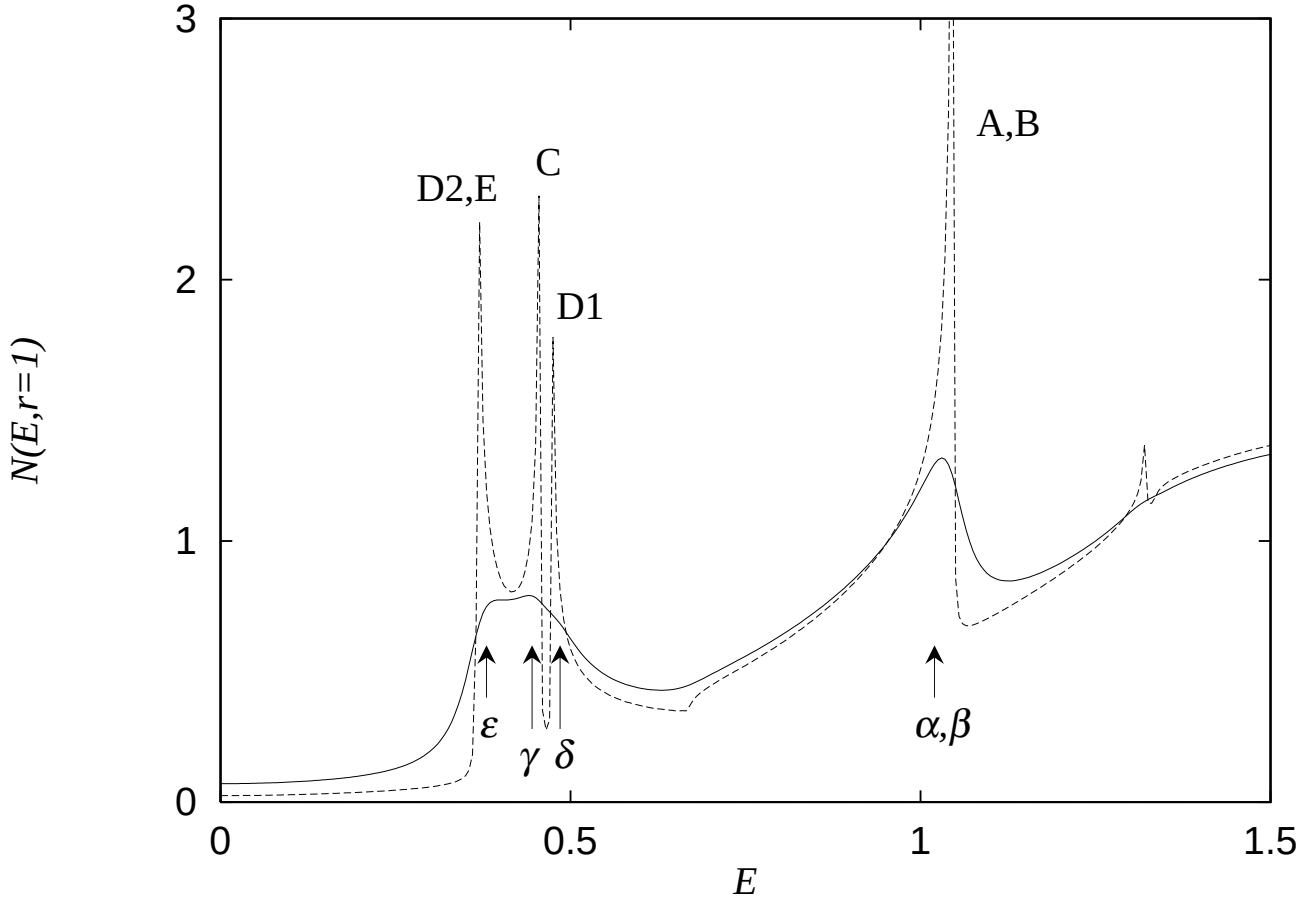

Fig. 5(c)

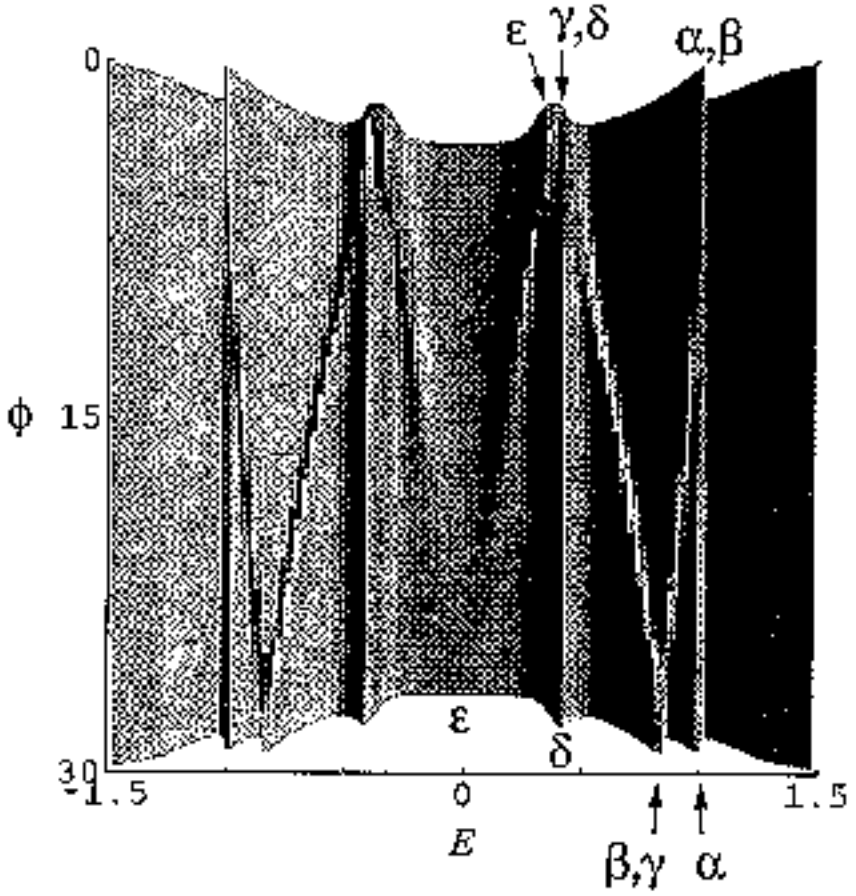

Fig. 6

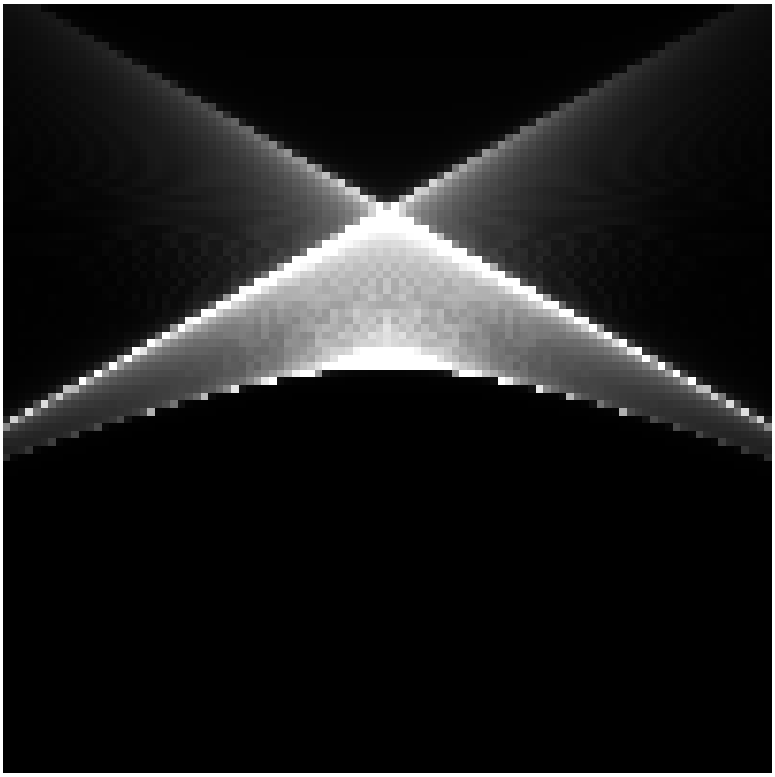

Fig. 7

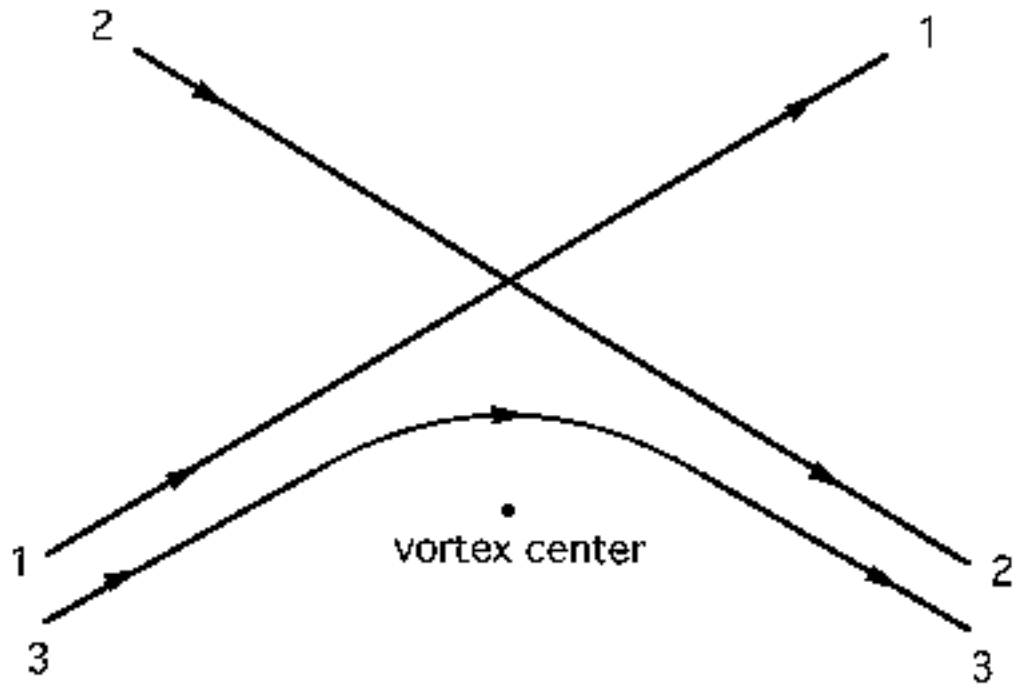

Fig. 8

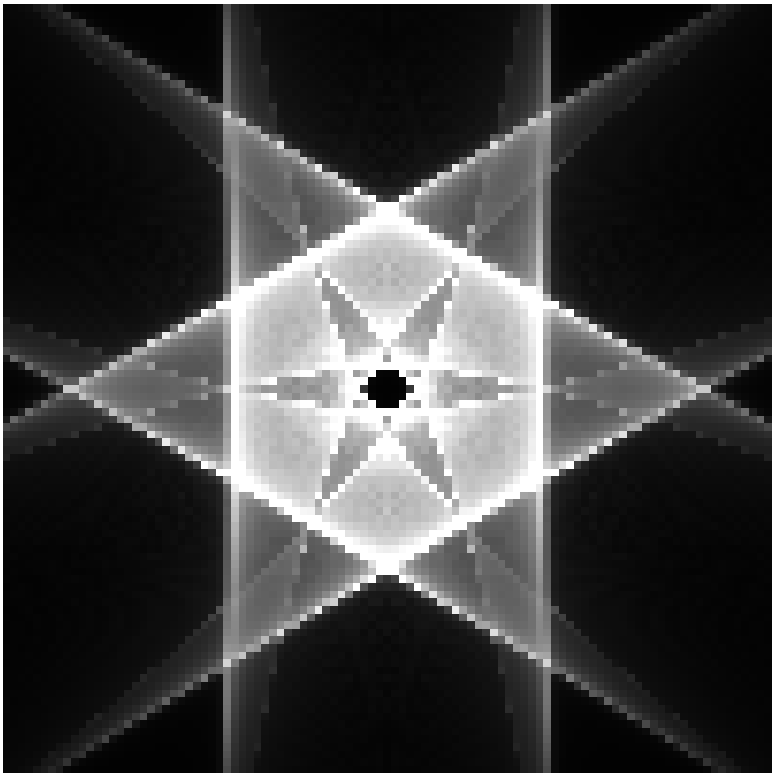

Fig. 9

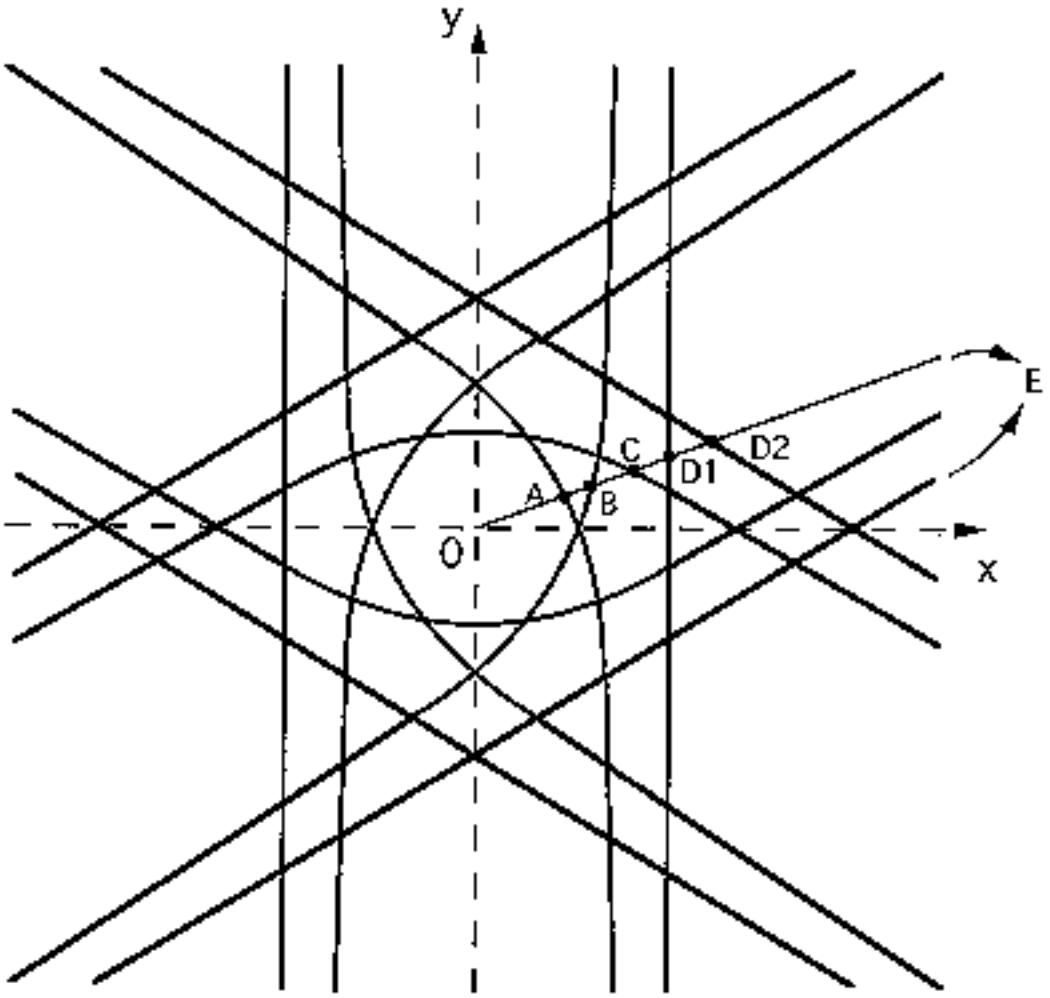

Fig. 10

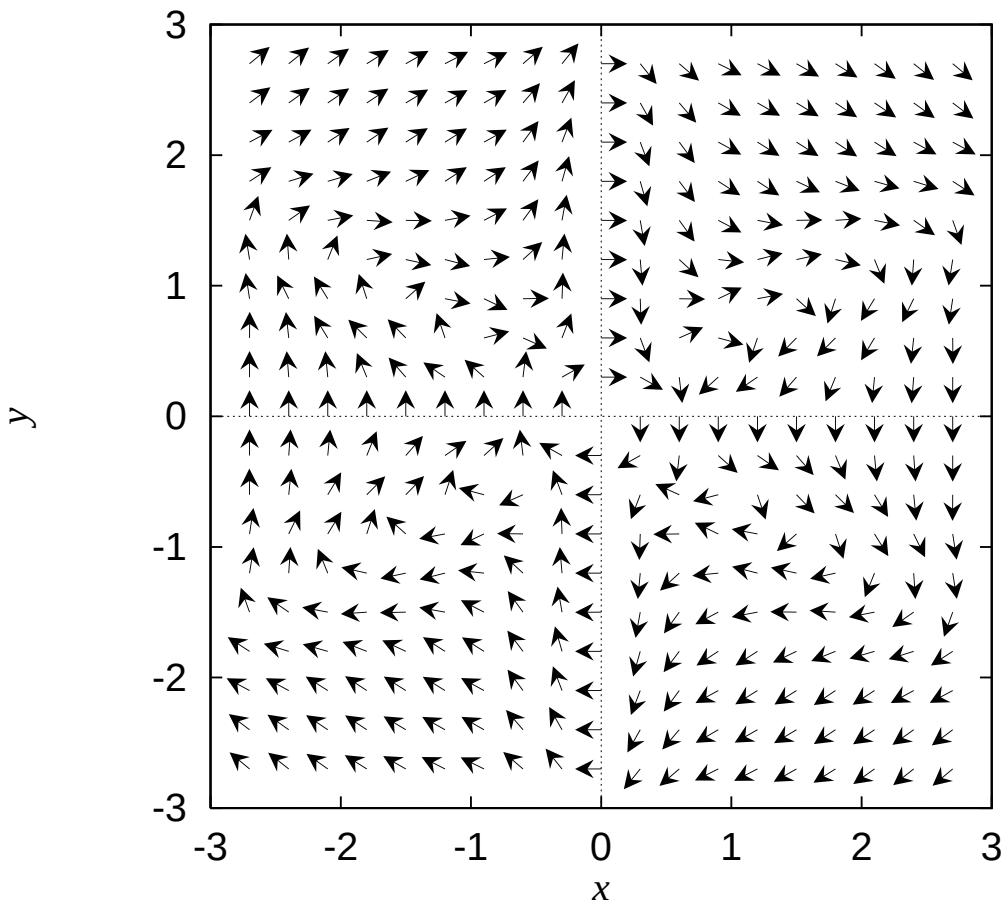

Fig. 11(a)

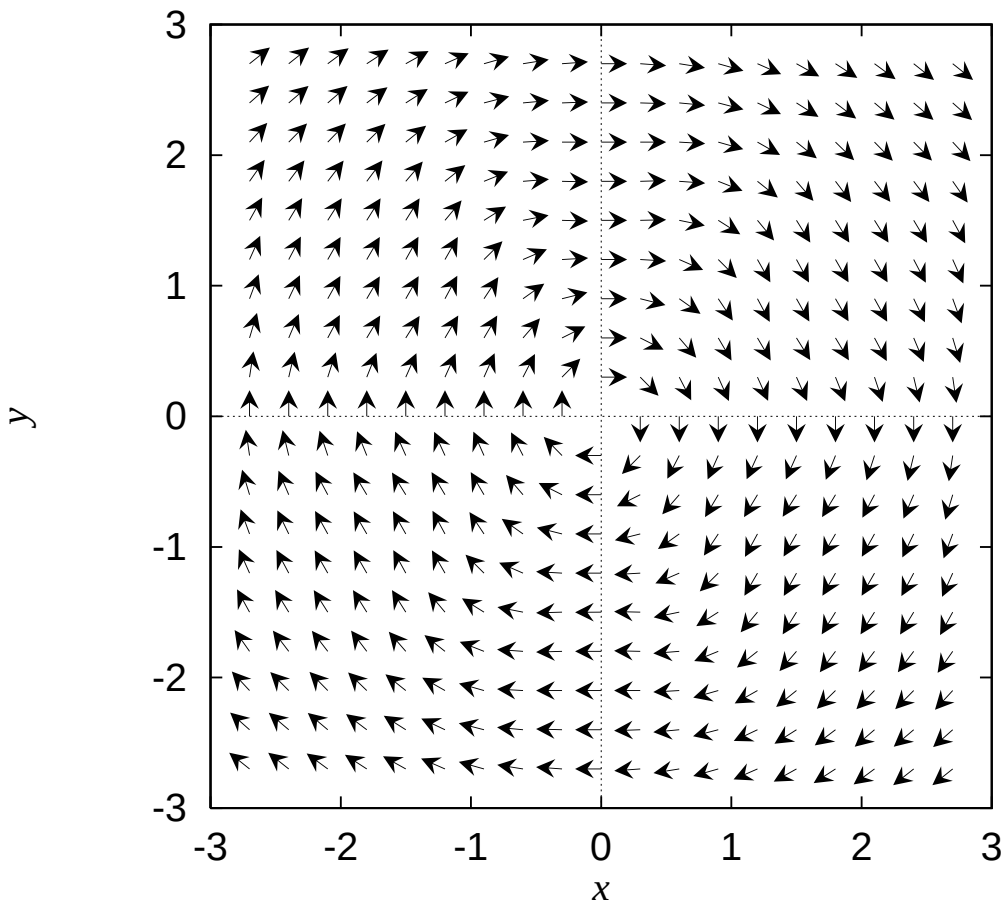

Fig. 11(b)

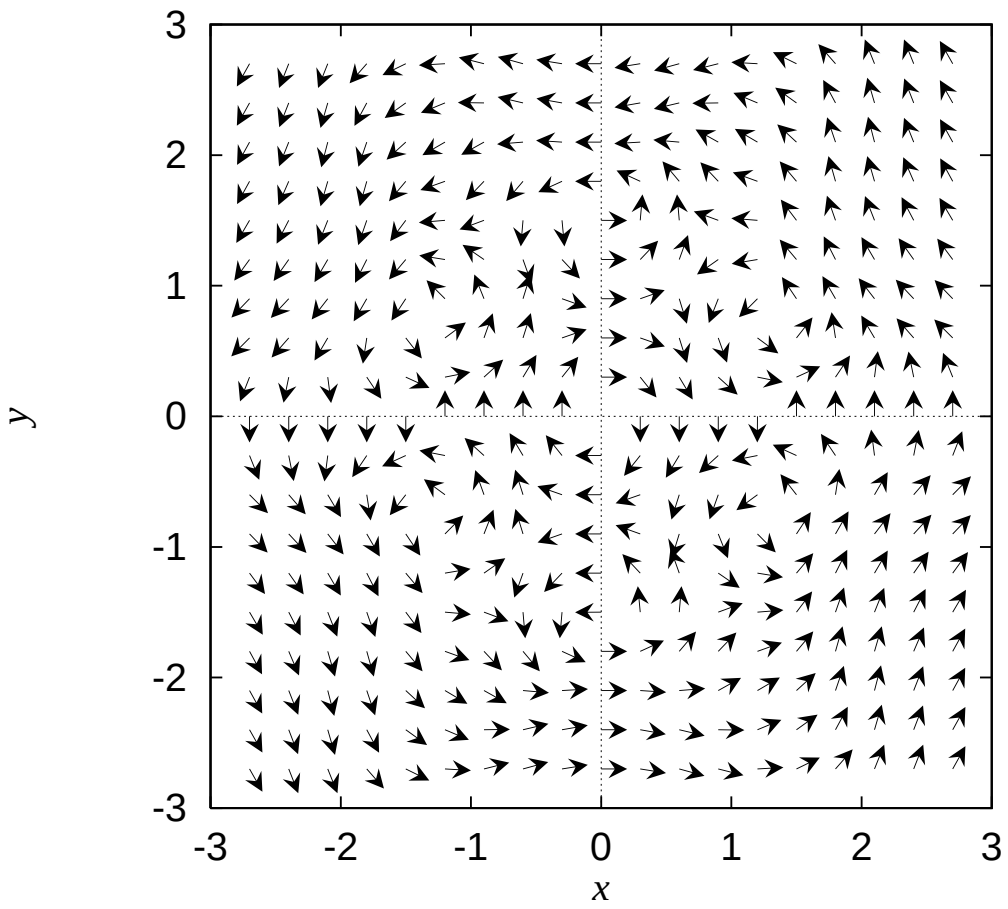

Fig. 11(c)

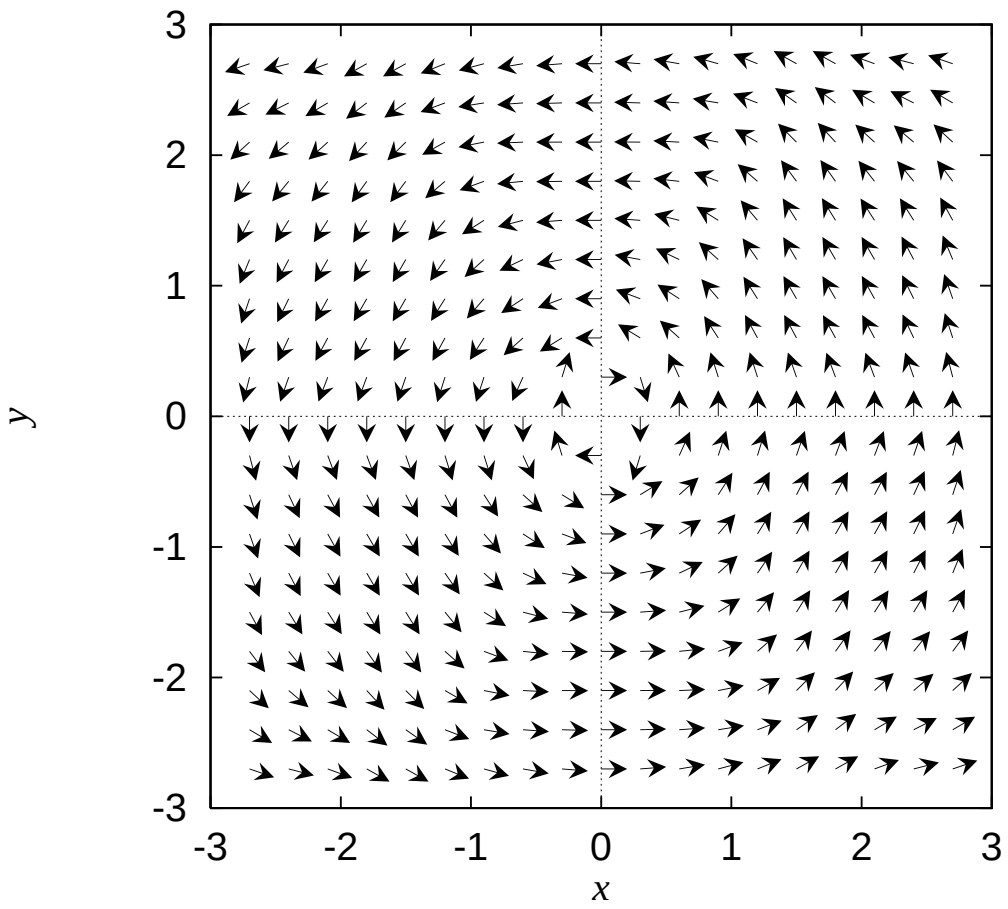

Fig. 11(d)